Published in final edited form as:
J Comp Neurol. 2014 February ; 522(2): . doi:10.1002/cne.23398.

IB4-binding sensory neurons in the adult rat express a novel 3′ UTR-extended isoform of *CaMK4* that is associated with its localization to axons

Benjamin J. Harrison[1,2], **Robert M. Flight**[1], **Cynthia Gomes**[4], **Gayathri Venkat**[1,2], **Steven R Ellis**[4], **Uma Sankar**[6,7,8], **Jeffery L. Twiss**[5], **Eric C. Rouchka**[9], and **Jeffrey C. Petruska**[1,2,3]

[1]Anatomical Sciences and Neurobiology, University of Louisville, Louisville, Kentucky, 40202, USA

[2]Kentucky Spinal Cord Injury Research Center (KSCIRC), University of Louisville, Louisville, Kentucky, 40292, USA

[3]Department of Neurological Surgery, University of Louisville, Louisville, Kentucky, 40202, USA

[4]Department of Biochemistry and Molecular Bi ology, University of Louisville School of Medicine, Kentucky, 40202, USA

[5]Department of Biology, Drexel University, Philadelphia, Pennsylvania, 19104, USA

[6]James Graham Brown Cancer Center, University of Louisville, Louisville, Kentucky, 40292, USA

[7]Owensboro Cancer Research Program, University of Louisville, Owensboro, KY 42303, USA

[8]Department of Pharmacology and Toxicology, University of Louisville, Louisville, Kentucky, 40292, USA

[9]Department of Computer Engineering and Computer Science, University of Louisville, Louisville, Kentucky, 40292, USA

Abstract

Calcium/Calmodulin-dependent protein Kinase 4 (Gene and transcript: *CaMK4*; Protein: CaMKIV) is the nuclear effector of the Ca^{2+}/Calmodulin Kinase (CaMK) pathway where it co-ordinates transcriptional responses. However, CaMKIV is present in the cytoplasm and axons of subpopulations of neurons, including some sensory neurons of the dorsal root ganglia (DRG), suggesting an extra-nuclear role for this protein. We observed that CaMKIV was expressed strongly in the cytoplasm and axons of a subpopulation of small diameter DRG neurons, most likely cutaneous nociceptors by virtue of their binding the isolectin IB4. In IB4+ spinal nerve axons, 20% of CaMKIV was co-localized with the endocytic marker Rab7 in axons that highly expressed CAM-Kinase-Kinase (CAMKK), an upstream activator of CaMKIV, suggesting a role for CaMKIV in signalling though signalling endosomes. Using fluorescent in situ hybridization (FISH) with riboprobes, we also observed that small diameter neurons expressed high levels of a novel 3' untranslated region (UTR) variant of *CaMK4* mRNA. Using rapid amplification of cDNA ends (RACE), RT-PCR with gene-specific primers, and cDNA sequencing analyses we determined that the novel transcript contains an additional 10kb beyond the annotated gene terminus to a highly conserved alternate poly-adenylation site. qPCR analyses of fluorescent-activated cell sorted (FACS) DRG neurons confirmed that this 3'UTR-extended variant was

Corresponding Author: Jeffrey C. Petruska, University of Louisville, Louisville, Kentucky, 40202, USA. Ph: 1-502-852-8057 j.petruska@louisville.edu.

Conflict of Interest Statement The authors declare that they have no conflict of interest.

preferentially expressed in IB4-binding neurons. Computational analyses of the 3'-UTR sequence predict that UTR-extension introduces consensus sites for RNA-binding proteins (RBPs) including the Embryonic Lethal Abnormal Vision (ELAV)/Hu family proteins. We consider the possible implications of axonal CaMKIV in the context of the unique properties of IB4-binding DRG neurons.

Keywords

sensory neuron; pain; signal transduction; alternate polyadenylation; CLIP-seq; neural plasticity; RNA-binding proteins; dorsal root ganglion

Introduction

Responses to variations in intracellular Ca^{2+} modulate a multitude of processes and are mediated by Ca^{2+} sensor molecules such as calmodulin that interact with transducer molecules including the calcium/calmodulin-dependent protein kinases (CaMKs). Ca^{2+}/calmodulin-dependent protein kinase 4 (Gene and transcript: *CaMK4*; Protein: CaMKIV) is a member of the CaMK family with its protein product predominantly localized to the nucleus. It is best known for its role in phosphorylating and activating calcium response-element binding (CREB) protein to regulate gene transcription (Wayman et al., 2008), and in regulating alternate splicing through its interaction with ribonuclear protein L (Yu et al., 2009). In the nervous system CaMKIV regulates specific modes of plasticity. For example, in the hippocampus and cerebellum it is required for long term depression (LTD), dendritic growth, and the acquisition of memories (e.g.: Ahn et al., 1999; Boyden et al., 2006; Kang et al., 2001; Redmond et al., 2002). CaMKIV entrance into the nucleus requires both interaction with the adapter protein importin-α (Kotera et al., 2005) and activation of the kinase domain mediated by CaMK-kinases (Lemrow et al., 2004). However, concentrations of CaMKIV immunoreactivity distal to the soma in dendrites and/or in axons in specific populations of neurons have previously been described (Jensen et al., 1991; Nakamura et al., 1995), including in the sensory axons of dorsal root ganglion (DRG) neurons (Ji et al., 1996). CaMKIV is actively transported along axons of the sciatic nerve in both retrograde and anterograde directions (Ji et al., 1996) and there is ultrastructural evidence that this protein locates within vesicles in CNS axons and synapses (Jensen et al., 1991; Nakamura et al., 1995). Taken together, these works suggest that there may be extra-nuclear functions of CaMKIV that have not been described.

The DRG houses diverse populations of neurons with distinct anatomical, electrophysiological, and neurochemical characteristics (e.g., Lawson, 2002; Petruska et al., 2000 b). Characterization of expression patterns of proteins within those populations can provide insight into the neurological role of said protein and insight into the means by which the different neurons carry out their functions. Characterising classes of neurons with differences in the subcellular distribution of the CaMKIV protein may therefore offer some indication as to its extra-nuclear role in those neurons. Ji et al. (1996) observed a striking amount of non-nuclear CaMKIV immunoreactivity in approximately 30% of DRG neurons, nearly all of which were small or medium in diameter. In that study, elevated non-nuclear immunoreactivity was found in approximately 25% of the calcitonin gene-related peptide (CGRP)-expressing population and in the majority of somatostatin (SOM)-expressing populations (Ji et al., 1996). The determination of which populations of DRG neurons expressed non-nuclear CaMKIV nevertheless remained incomplete. Given the size profile of neurons displaying non-nuclear CaMKIV, and the fact that only 25% of those were found in the CGRP-expressing population, we hypothesized that perhaps the population expressing non-nuclear CaMKIV might be the same as the population binding the isolectin B4 (IB4)

from *Bandeiraea simplicifolia* (formerly *Griffonia simplicifolia*). IB4-binding is a positive marker of the subpopulation of small-diameter DRG neurons often defined by their lack of expression of most neuropeptides (i.e., non-peptidergic) (Wang et al., 1994). However, IB4-binding is not restricted to the non-peptidergic neurons, with nearly 50% overlap between the CGRP-expressing and IB4-binding populations in rat (Wang et al., 1994). The somatostatin (SOM)-expressing population is entirely encompassed inside of this junctional population displaying both CGRP-expression and IB4-binding (Wang et al., 1994). We therefore sought to determine the distribution of non-nuclear CaMKIV immunoreactivity within the IB4-binding population of DRG neurons. This population gives rise to unmyelinated axons (Streit et al., *1*985; Wang et al., 1998a) that predominantly innervate cutaneous targets and some visceral targets, with little innervation of muscle (Bennett et al., 1996; Petruska et al., 1997; Wang et al., 1998 a; b), and display properties consistent with nociceptive functions (Fang et al., 2006; Petruska et al., 2000 a; b).

Methods

Materials

All chemicals and reagents were obtained from Sigma-Aldrich unless otherwise stated. Ultra-pure biochemistry-grade chemicals were used wherever possible.

Animals

All animal procedures were approved by the Institutional Animal Care and Use Committee of the University of Louisville consistent with federal regulations and guidelines. *CaMK4* germline knock-out (*CaMK4*-KO) mice were developed using a targeting vector that replaced exons 1 and 2 with a neomycin cassette as described by Wu et al., (2000).). These mice were maintained in house and used for antibody validation studies (Figure 1). All other experiments were performed using Sprague Dawley rats (Taconic, New York).

PC12 Cell Transfection and Protein Extraction

PC12 cells were maintained in suspension in RPMI-1640 media supplemented with 10% heat-inactivate horse serum and 5% foetal-bovine serum. Cells were transfected after adhering overnight onto collagen coated plates at a density of 10,000 cells/cm^2. All plasmids were obtained from the Open Biosystems clone library (*CaMK1* = #7098592, *CaMK2* = #7939424, *CaMK4* = #7455982). Cells were transfected with 1μg of plasmid DNA and 5μl of Lipofectamine-2000 (Invitrogen) per ml of culture medium according to the manufacturer's instructions. Transfection commenced for 18 hours in growth media when the cells were washed with PBS and scraped into 1.5ml centrifuge tubes with 1ml of cold PBS before sedimenting them at 400g for 4 minutes at 4C. Cells were then lysed using RIPA protein extraction buffer containing complete mini-protease inhibitor tablets (Roche) for 10 minutes on ice with intermittent agitation. Lysates were cleared twice at 12000g for 15 minutes at 4C before determination of protein concentration using the Bradford method (Biorad).

Western Blotting

Western blotting was performed according to Harrison et al., (2008) with the following modifications: 20μg of DTT-reduced protein was loaded per lane into 4–12% gradient Novex (Invitrogen) PAGE gels. Following electrophoresis, protein was transferred onto nitrocellulose membranes in 1X Tris-glycine buffer with 0.1% SDS and 20% methanol. Membranes were blocked for 1 hour in antibody dilution buffer (phosphate-buffered saline (PBS) containing 0.05% Tween-20 and 5% non-fat milk) with constant shaking before incubation overnight at 4C with primary antibody in dilution buffer (Table 1). Membranes

were then washed with PBS with 0.05% Tween-20 (PBS-T) before incubation with HRP-conjugated secondary antibodies (Jackson ImmunoResearch) diluted 1:5000 in dilution buffer. Protein was detected with enhanced chemiluminescence (ECL) and photographic film according to standard protocols.

Immunofluorescence

Antibody Characterization—See Table 1 for a list of all antibodies used. See Figure 1 for characterisation of the CaMKIV antibodies.

The pan-CaMKK antisera detected WB signals for CaMKK isoforms that were abolished by germ-line deletion (Green et al.,2011, Lin et al.,2011).

The Rab7 antisera was used as an endosomal organelle marker that colocalised with fluorescent tagged exogenous Rab7 protein (Dobrowolski et al.,2012, Humphries et al., 2011).

The CGRP antisera has been extensively used for identifying peptidergic peripheral sensory neurons in rats. For example, CGRP staining in rat spinal cord and DRG was abolished by preabsorption with the CGRP peptide (Brumovsky et al.,2002).

The pan-CaMKI antisera recognised a band on Western blot of appropriate size that was specifically reduced in conjunction with reduced CAMKI mRNA (Jiao et al.,2009). CaMKI overexpression in PC12 cells caused an increase in of a band of the same size (Figure 1).

The pan-CaMKII antisera recognises bands in Western blot of appropriate sizes for CaMKII isoforms (Figure 1). CaMKII δ overexpression in PC12 cells caused an increase in a band of appropriate size (Figure 1).

The GAPDH antisera has been extensively used as a loading control for Western blots. As expected, it detected a single band at the appropriate molecular weight (Figure 1).

Tissue Sample Preparation, Sectioning and Staining—DRG were dissected with 2mm of adjoining intact spinal nerve from adult animals and prepared for sectioning as in Petruska et al. (2000b). Briefly: Samples were fixed in 4% paraformaldehyde in PBS for 30 minutes before cryoprotection by incubating overnight in 30% sucrose. 12–16μm sections were cut using a cryostat and mounted onto gelatin/poly-L-lysine substrated slides. Sections were stained according to Petruska et al. (2000b) with the following changes: Sections were blocked and delipidated simultaneously by incubation with 4% donkey serum in PBS containing 0.4% Triton-X100 for 1 hour at room temperature. Primary antibodies (Table 1) were diluted in blocking buffer and applied to sections overnight at room temperature before washing 4 times for 5 minutes with blocking buffer. Fluorophore conjugated highly cross-adsorbed secondary antibodies (Jackson ImmunoResearch) were diluted 1:200 in blocking buffer and applied to sections at room temperature for 3 hours before the same washing procedure. For IB4 staining, biotin-conjugated IB4 was used at 1:50 dilution and detected with Pacific Blue-conjugated streptavidin (Invitrogen) at 1:50, which was rinsed off of sections with PBS after 30 minutes. Slides were cover-slipped with antifade-containing medium (ProLong® Gold; Invitrogen) and allowed to set overnight.

Epifluorescence Microscopy and Quantitative Analysis of DRG Neuron Fluorescence Intensity—Multichannel fluorescent micrographs of entire longitudinal DRG sections were obtained using an Nikon eclipse Ti inverted microscope with 10X objective and automated field stitching on Nikon Elements software. Two sections per animal containing more than 200 neurons with visible nuclei were selected from 4 animals.

Sections were spaced more than 50μm apart to ensure that no single neuron could be included in the analysis twice. Using Elements software, individual neurons with visible nuclei were then manually circled to generate separate regions of interest (ROIs). Mean fluorescent intensities for IB4, CGRP and CaMKIV were recorded along with the mean neuronal diameter from each ROI. All ROI data from both sections from individual animals were then collated into a single data set per animal, yielding data from over 400 neurons per animal. The median staining intensity for each channel was then calculated for each of the 4 data sets (i.e., the median intensity of each DRG) to allow for normalization of fluorescence intensities to the mean median value (division by central tendency (median) method). Firstly, to observe the distribution of CaMKIV expression according to neuron soma size, normalised data from all animals were collated into a single data set and subsequently binned according to soma diameter (2μm bin sizes). The sum CaMKIV intensity was then calculated in each bin (grey bars Figure 3A). This sum CaMKIV expression signal was subsequently split into 4 populations according to $CGRP^{+/-}/IB4^{+/-}$ staining (black bars Figure 3A). Secondly, to determine mean per-animal CaMKIV expression in each of the four populations according to traditional size divisions, neurons were assigned to either small (0–35μm), medium (36–50μm) or large (51+μm) populations. These size divisions were chosen due to the well-established somatosensory characteristics that vary according to neuron diameter. Then, the mean CaMKIV fluorescence intensity was calculated in each category for each rat (Figure 3B). Mean per-rat intensities were then compared using one-way ANOVA with Tukey's post-hoc tests. For correlation analyses, normalised fluorescence intensity data from all animals were collated into a single data set (Figure 3C) and the Pearson's r correlation coefficient calculated.

Antibody Preadsorption with Mouse Brain Lysates—Fresh whole adult single mouse brains from wild type or $CaMKIV^{-/-}$ mice were homogenized in 20ml of RIPA buffer on ice using a Polytron rotor-stator using short bursts in centrifuge tubes on ice. After complete disruption, homogenate was spun at 13,000 g for 5 mins in 1.5ml aliquots and the pellets discarded. Lysate protein concentration was determined using the Bradford method before flash freezing and storage at −80°C. For preadsorption, protein was added to rabbit antiserum diluted 1:400 (final antibody concentration of 0.25ng/μl, protein concentration of 0.1125mg/ml) in antibody dilution buffer for 30 minutes at room temperature. Following incubation, preadsorbed antibody samples were incubated on mounted DRG sections, prepared and blocked as above, overnight at room temperature in humidity chambers. Slides were then washed and antibody binding detected using fluorophore conjugated secondary antibodies as above.

High Magnification Confocal Microscopy and Sub-Cellular Colocalisation Analysis—A Nikon C1 confocal microscope system with a 60X objective of NA 1.4 was used to collect all confocal micrographs. For imaging axons in spinal nerve sections, Z-stacks were collected at 200nm intervals, +/− 1μm for a total of 11 planes/field with the pinhole set as small as possible (30nm). The zoom setting was set to sample the X/Y plane at the Nyquist rate (1024×1024 pixels, zoom X2.83 = 74nM/pixel). To determine mean CaMKIV intensities in IB4 axons, single Z-slices from 3 random fields were used. In each slice, IB4+ axons were isolated by magic wand selection in Adobe Photoshop v12.0.4 after background subtraction and thresholding of the IB4 channel. Mean CaMKIV intensities were then calculated inside and outside IB4+ axons by exporting the selections to the Fiji package of ImageJ v1.43 (Schindelin et al., 2012) and using the measurement tool (data in Figure 5). For presentation, Z-stack median intensity projections were deconvolved with predicted spread point function (SPF) images generated using the SVI webtool (http://www.svi.nl/NyquistCalculator). The Richardson-Lucy deconvolution algorithm (Holmes and Liu, 1989) was employed by using deconvolve-lab in Fiji (Projections in Figure 6). For

3D rendering, Z-stacks were inputted into bioimageXD v1.0 software (Kankaanpää et al., 2012). IB4 was volume rendered and protein inside axons was visualized by surface rendering (3D rendering in Figure 6). Z-stacks containing CaMKIV and Rab7 signals were inputted into bioimageXD software for 3D colocalisation assessments. Thresholds and Pearson's correlations were calculated according to the method of Costes (Costes et al., 2004). Mean % CaMKIV signal colocalisation was determined from 3 random fields.

Micrograph Image Preparation—Micrograph images were adjusted for brightness and contrast with Adobe PhotoShop version 10.0.1. Plates were assembled and annotated in Microsoft PowerPoint 2013 in 300dpi.

Fluorescence-Activated Cell Sorting (FACS) of IB4+ DRG Neurons

For each replicate experiment, all DRGs from two 4-week old rats were pooled for dissociation as follows. Ganglia were harvested in colourless DMEM/F12 media in 1.5ml Eppendorf tubes before transferring into a 50 ml conical tube for washing with colourless DMEM/F12/PenStrep media 6 times. After the final wash all media was removed and 2.5ml of proteinase media (5mg/ml dispase and 2mg/ml collagenase in DMEM/F12) was added. Tubes were then incubated for 30 minutes with constant swirling at 37C before replacing the media with 2.5 ml of fresh proteinase media and incubation for a further 15 minutes with constant swirling. The proteinase media was then completely removed and DRGs washed once with colourless DMEM/F12. The wash media was then completely removed before addition of 1ml of DMEM/F12 supplemented with 10% FBS and 1% N2 and titurated 15–20 times with a flame polished Pasteur pipette to develop a single cell suspension. Cells were then sedimented for 5min at 400g and the supernatant removed. Dissociated cells were then split into 2 tubes, one for staining with FITC-conjugated IB4, the other as a negative staining control. Cells were stained for 20 minutes in colourless DMEM/F12 containing 1:100 v/v FITC-IB4 at room temperature with constant gentle agitation before spinning at 200g for 4 minutes and washing 3 times with colourless DMEM/F12 at room temperature. FACS gates were set with the negative staining control cells to allow subsequent sorting of FITC+/− cell populations directly into Trizol RNA extraction reagent (Invitrogen).

Determination of CaMK4 Transcript Variant Expression in IB4+ Neurons

RNA from FACS sorted cells was extracted from Trizol reagent per manufacturer's instructions. To ensure purity of RNA, RNA isolates were subsequently applied to genomic DNA eliminator columns (Qiagen) before RNA concentration through mini-prep columns as per manufacturer's instructions. RNA quality control, reverse transcription and qPCR were performed according to Hill et al., (2010). Briefly, 250ng of RNA input was used to generate cDNA template with Quantitect reverse transcriptase mastermix containing a mixture of oligo(dT) and random primers. This primer mix ensured that long transcripts would be reverse transcribed. PCR reactions were performed with 5ng input cDNA in triplicate using 2X SYBR green master mix (Roche). qPCR was performed with SYBR green detection using a Corbett Rotorgene instrument with the following cycle parameters:1) hotstart for 10 mins at 95C, 2) cycle: 95C for 30 seconds, anneal/extend for 60s at 60C. SYBR green fluorescence was determined at the end of each extension.

qPCR Probe Design—PCR amplicons for SYBR green detection were generated using PerlPrimer software v1.1.21 (Marshall 2004). Wherever possible, probes were designed with the following parameters: 1) Spanning exon boundaries to reduce noise from genomic DNA, 2) small size (80–150 bp) to increase amplification efficiency, 3) including a G/C clamp to reduce miss-priming, 4) 45–55% G/C content to optimise amplification efficiency, 5) melting temperatures of 60C +/− 2C and 6) between 18–24 nucleotides in length. Candidate probes were pre-screened for potential non-specific amplification using the ePCR tool on the

NCBI website before the amplification efficiency of all probes determined by standard curve analysis. Only probes with amplification efficiencies above 95% were used (Table 2).

Computational Prediction of Alternate Polyadenylation (APA) Sites

The POLYAR algorithm Akhtar et al., (2010) was used to predict APA sites downstream of the *CaMK4* stop codon to the distal-most expressed sequence tag (EST) cluster identified with the UCSC genome browser. Only polyadenylation sites (PASs) containing consensus upstream and downstream elements and with W-scores above that of the canonical site (termed “PAS-strong” sites) were considered for validation.

3' Rapid Amplification of cDNA Ends (3'RACE)

RNA pooled from adult rat DRGs was used as a template for reverse transcription primed with anchored (or “lock-docking”) oligo(dT) primer with an adaptor sequence (Table 3: RT Primer) (Borson et al., 1992). The resulting cDNA template pool was then inputted into PCR with specific forward primers designed approximately 500bp upstream of the APAs predicted by POLYAR (Table 3: RACE_A-G) with the adaptor sequence used as the reverse primer (Table 3: Adaptor primer) and amplified using Taq polymerase (Qiagen). The following thermocycle parameters were used:1) hotstart for 10 mins at 95°C, 2) Cycle: 95°C for 30 seconds, anneal/extend for 60s at 60°C. PCR reactions were then separated on 1.2% agarose gells. All observed PCR products regardless of size were isolated using Qiagen gel purification columns according to the manufacturer's instructions. PCR products were then sequenced using the corresponding RACE forward primers (Table 3). Obtained sequences were then aligned to the rat genome (ver rn4) using the BLAT feature of the UCSC genome browser (Kent et al., 2002).

Assessing UTR Contiguity Using Gene-Specific Primers (GSPs) During cDNA Synthesis

Reverse transcriptases operate in the 3' to 5' direction and require double stranded RNA-DNA hybrids for priming. Most often cDNA synthesis is achieved using oligo(dT) or random oligomer primers. For our purposes here we designed a sequence-specific primer to generate specific cDNA templates (i.e., only those transcripts containing the sequence of interest are converted to cDNA) in continuity with the primed sequence (which we presumed to be an extended UTR variant). To determine if the 3'predicted UTR was contiguous with the *CaMK4* coding region (CDS), gene specific primer s (GSP, sequence: ACCGCCATCATAACATACCC) were employed to synthesise cDNA from DRG total mRNA using Superscript3 reverse transcriptase (Invitrogen). Reverse transcriptases have an inherent on/off rate and as such dissociate from ongoing cDNA synthesis more frequently as the length of cDNA increases. We therefore designed a gene specific reverse transcription primer mapping within the center of the putative 3' extension, approximately 4000 nucleotides downstream of the *CaMK4* stop codon within an EST cluster, ensuring the region of interest would be “in-range” of the RT enzyme. This primed the reverse transcriptase reaction specifically within the putative extended UTR of the transcript only (i.e,. all other mRNA species in the reaction not attached to the putative *CaMK4* UTR were not made into cDNA). Then, to determine if the CDS is contiguous, PCR primers were designed to probe the entirety of the coding region in 800bp fragments (Table 4). cDNA synthesis reactions without primers were performed to control for non-specific RT priming. Following this the entire transcript was sequenced and the resulting contigs assembled for sequence analysis.

In situ hybridisation

All procedures were carried out under strict RNAse-free conditions. All equipment, work areas, instruments and consumables were either purchased and maintained as certified RNAse-free or were decontaminated using RNase-away cleaning reagent (Ambion).

Rats were exsanguinated and fixed with transcardial 4% PFA in PBS at 4°C. DRG with connected spinal nerves were immediately removed from rats and post fixed for 15 minutes in cold 4% PFA in PBS on ice. Fixative was then removed and DRGs were incubated overnight at 4°C in RNA-safe cryoprotectant (autoclaved 30% sucrose in PBS supplemented with DEPC). The following morning, DRGs were snap frozen in tissue freezing media, wrapped in aluminium foil, and stored at −80C in airtight 1.5ml tubes until required for sectioning. 14μm sections were then cut using a cryostat under RNase-free conditions. Sections were collected onto Superfrost Plus Gold slides (Fisher) for firm adherence.

Riboprobes were synthesised by *in vitro* transcription of plasmids linearized using restriction digestion. All plasmids were obtained from the Open Biosystems clone library. A rat *CaMK4* plasmid (Open Biosystems # 7455982), digested with Sma1, was used to generate antisense probes for the canonical transcript of *CaMK4*. This digestion site was chosen to map to the C-terminal domain of CaMKIV that is unique to this family member and thus reducing the potential of cross reaction with other CaM kinases. A plasmid containing an EST mapping within the 3'UTR (Open Biosystems #7384459), digested with Sma1, was used to generate antisense probe specific for the 3'-extended *CaMK4* variant. Same-sense negative control riboprobe was synthesised with SP6 RNA using the CDS plasmid digested with Xho1.

Linearised plasmids were purified by phenol:chloroform extraction before *in vitro* transcription using a Digoxigenin labeling kit (Roche) according to the manufacturer's instructions. Unincorporated nucleotides were removed. Probe size was then reduced by alkaline hydrolysis in 40mM NaHCO3, 60mM Na2Co3 buffer at 60°C for 90 minutes to increase penetration of the probe into tissue sections. The efficiency of probe synthesis and hydrolysis was determined by formamide PAGE. Probe was hybridized to sections as described by Muddashetty et al., (2007). Slides were then blocked with 4% BSA in PBS with 0.1% TritonX100. Digoxigenin-labeled hybridised probes were detected by incubation with Cy3-labeled mouse anti-DIG antibody (Jackson ImmunoResearch) diluted 1:200 in PBS containing 1% BSA and 0.1% triton.. Sections were imaged using confocal microscopy.

Characterisation of the Novel CaMK4 3'UTR-Extended Variant

Genomic positions of the rat, mouse and human 3'UTR extension—Genome assemblies used were: rat (Rn 5), mouse (Mm 10), and human (Hg 19). Matching regions in mouse and human were defined based on the results of a BLAT query of the rat sequence against the mouse and human genomes. DNA sequences from the specified regions were obtained from UCSC genome browser: http://genome.ucsc.edu/cgi-bin/hgc?o=7512442&g=getDna&db=rn5, changing “db” as required to the appropriate genome code (above). The corresponding rat, mouse and human genomic positions are shown in Table 5.

Identification of RNA-Binding Protein Sites—Position weight matrices (PWMs) for 72 RNA-binding proteins (all species) were bulk downloaded from the RNA-binding protein databank (Cook et al., 2010). The matchPWM function in v2.24.1 of the Biostrings Bioconductor package was used to predict binding sites in the *CaMK4* 3' UTR of rat, mouse and human (Table 6).

Identification of Conserved Regions—Homologous regions in the 3' UTR of *CaMK4* across all three species was determined using two different methods. BLAT was used to identify homologous blocks of sequence in a pairwise fashion, by comparing the rat sequence to the mouse and human sequences, and comparing the mouse with human. For a finer result, a three way alignment of the sequences was performed using the EBI web server

version of Clustal omega (Sievers et al., 2011). Regions of homology are defined as runs of at least 8 bases, where either the rat or mouse sequence matched the human, without any gaps in any of the three sequences.

Mapping Elavl1 RIP-seq Data—Conversion between coordinates in genome builds was performed using the UCSC LiftOver tool (Hickey et al., 2013). Elavl1 protein binding interval data came from ENCODE project (De Souza 2012) RIP-seq peak data hosted at the UCSC genome browser ENCODE portal.

Determination of ELAVL1 Binding-Site Coverage—To determine if the observed number of ELAVL1 binding sites in the *CaMK4* UTR was greater than the number in other gene UTRs, coverage of Elavl1 binding in 3'UTRs was determined for 2000 randomly selected Ensembl transcripts. 3' UTRs for the transcripts were determined based on the transcription and coding start and stop sites defined in the Ensembl gene track from the UCSC genome browser. Coverage was calculated as the number of bases in the 3'UTR intersected by regions from the binding data, divided by the total number of bases in the 3'UTR.

Results

Specific Detection of CaMKIV in Adult Rodent DRG

To reliably detect CaMKIV protein in histological DRG sections, we initially screened 2 rabbit antisera indexed in the Human Protein Atlas (Cat#s HPA011753, HPA017206) in addition to a mouse monoclonal antibody (BD Biosciences; Cat# BD610275). In our hands antibody HPA011753 did not work on sections of rat DRG (data not shown), possibly because it was generated using a Human-derived antigen mapping to a C-terminal region only 50% homologous to the rat amino acid sequence. The other antisera (HPA017206 and BD610275) displayed positive staining in sections of rat DRG and were subject to further assessment. The selected rabbit antisera (HPA017206) was raised using an antigen corresponding to a region encompassing the end of the catalytic domain and the autoinhibitory and calmodulin-binding domain (AI/Cam). The mouse antibody is raised against an adjacent protein region that included the N-terminal region (Figure 1A).

The gold standard method for antibody validation is to provide a situation where the antigen has been specifically removed from a matrix containing all potential non-specific binding sites. Mice with a germ-line deletion/interruption (KO mice) of the gene of interest can provide excellent material for this purpose. DRGs from CaMKIV KO mice were either homogenized for Western blot protein assays or sectioned for immunofluorescence studies (Figure 1 B–E). The signal from both antibodies was lost in Western blots, whereas signals from both pan-CaMKI and II antibodies appeared unaffected by CaMKIV knockout (Figure 1 C). Thus, these anti-*CaMKIV* antibodies can be used to specifically probe for CaMKIV in mouse protein lysates with no detectable cross-reaction with other CaM-kinases. Immunostaining with the rabbit antiserum on mouse tissues revealed staining similar to that previously observed staining rat tissue (Ji et al., 1996). A very sparse highly-punctate bright intra-nuclear staining pattern was observed in DRG sections of both WT and CaMKIV-KO mice (Figure 1D,E - arrows), indicating that this sub nuclear staining was not CaMKIV. A similar sparse punctate background staining was also observed using the rabbit antisera to stain sections of DRG tissue from rat (Figure 1F,K). However, this background signal was abolished by pre-incubation with mouse brain lysate from KO animals whereas the nuclear, cytoplasmic and axonal staining remained (Figure 1G). In contrast, signals from these sub-cellular compartments were uniformly diminished by pre-incubation with the same concentration of protein from the brain of WT mice (Figure 1H).

Noting that both map at least in part to conserved CaMK-family domain regions, we sought to determine if there was any cross reaction with these related proteins, of which CaMKI and II are the closest relatives. Using Western blotting, the size of the CaMKIV band (56Kda) was clearly different from that of CaMKI (45Kda) and 2 out of the 3 isoforms of CaMKII that we detected (50, and 65 kDa) allowing some CaMK family members to be differentiated by size alone (Figure 1I). CaMK1/2 plasmids transfected into PC12 cells did not cause an increase in non-specific signals with anti-CaMKIV antibodies, whereas enhanced CaMKIV signal was readily detected in lysates from the *CaMK4*/2-transfected PC12 cells (Figure 1I).

The immunogenic regions for the mouse and rabbit antibody are from largely distinct regions with only a small overlap (Figure 1A). Therefore, the chance that the mouse monoclonal and rabbit polyclonal immunoglobulins interact with similar epitopes is very small. In spite of this, both antibodies stained essentially identical structures in sections of rat DRG, aside from the above noted sub-nuclear background observed using the rabbit antibody (Figure 1J–L).

Taken together these assessments demonstrate that the CaMKIV-directed antibodies have little to no non-specific cross-reaction with other CaMK family members and validate the specificity of both antibodies for use in most Western blotting and immunofluorescence applications.

Distribution of CaMKIV protein in adult rat thoracic DRGs

The isolectin IB4 from *Bandeiraea* (formerly *Griffonia*) *simplicifolia* is used as a convenient positive marker for a subpopulation of small neurons and unmyelinated axons, many of which are cutaneous nociceptors, in rat and some other species. Used in conjunction with CGRP antisera, it is possible to identify the majority of neuropeptide-expressing (CGRP+/IB4+) and non-peptide expressing (CGRP−/IB4+) small-diameter neurons in sections of rat DRGs. It was evident from even a cursory examination of DRG sections co-stained for CaMKIV, CGRP and IB4 that there was a striking elevation of CaMKIV protein in IB4-positive neurons. CaMKIV was present at a high level in the nucleus, cytoplasm and axons in dorsal root (DR) and spinal nerve (SN) but not in axons within ventral root (VR) (Figure 2). We also observed the smaller subpopulation of neurons co-expressing CaMKIV and CGRP described by Ji et al., (1996). Four populations of neurons were defined based on expression of CGRP (+/−) and binding of IB4 (+/−) (Figure 2A–D). In $IB4^{-}$ cells, CaMKIV staining was weaker and largely restricted to the nuclei, whereas in $IB4^{+}$ populations CaMKIV was observed in the cytoplasmic and axonal compartments in addition to the nuclei.

To perform protein expression analyses, the CaMKIV fluorescent signal from stained sections of rat dorsal root ganglia was used to derive the relative protein expression level in given populations. As expected, we observed that the majority of CaMKIV signal was detected in small (88.7%) and medium (10.8%) diameter neurons. In the 4 co-stained populations, the majority of CaMKIV signal was detected in IB4+ cells (80.9%) (Figure 3A). Mean CaMKIV signal was significantly higher in IB4+ neurons by approximately 2-fold when compared to CGRP+/IB4− neurons and 3-fold when compared to CGRP−/IB4− neurons (Figure 3B). CaMKIV expression was highly correlated with increased IB4 expression (Figure 3Ci). In contrast, there is no such correlation when the *CaMKIV* immunoreactivity was compared to CGRP expression (Figure 3Cii). Intriguingly, in small diameter neurons mean CaMKIV expression was significantly greater in the CGRP−/IB4+ cells than in the CGRP+/IB4+ cells (Figure 3B) suggesting that neuropeptide expression correlates with lower CaMKIV in IB4+ cells.

We next sought to further characterize the subcellular distribution of CaMKIV in DRG neurons. Although axonal CaMKIV has been described in sensory nerve fibres (Ji et al., 1996), it has not been established which sub-population of neurons contain axonal CaMKIV. High magnification confocal imaging revealed a punctate staining throughout IB4+ nuclei, cytoplasm and axons (Figure 4). In spinal nerve, CaMKIV staining was significantly enriched in IB4 axons. IB4+ axons accounted for almost two thirds of the sum fluorescent signal intensity (Figure 5). As previously determined, 24 hours following sciatic nerve ligation CaMKIV accumulates on both the distal and proximal side of the ligature and so likely travels in both retrograde and anterograde directions (Ji et al., 1996). Numerous mechanisms exist to facilitate transporting protein cargo along sensory axons including direct association with motor protein complexes and transport within signaling endosomes (Fainzilber et al., 2011). To determine the extent of CaMKIV associated with retrograde signaling endosomes, we performed immunofluorescence colocalisation studies on spinal nerve sections co-stained with the endosome marker Rab7. Image analysis of confocal Z-stacks showed that Rab7 could clearly be detected in IB4 positive axons (Figure 6A–D). CaMKIV and Rab7 fluorescence intensities were significantly correlated in spinal nerve, where approximately 20% of the total CaMKIV signal was colocalised with Rab7 (Figure 6E–G,. Of this proportion of the total, approximately 75% was present within IB4+ axons (Figure 6H).

Axonal signaling endosomes are transport vesicles which contain components of a signaling cascade that allow the spatial redistribution of the initiating signal (Cosker et al., 2008). Having established that a significant proportion of CaMKIV was associated with Rab7 and therefore likely present within signaling endosomes, we also sought to determine if components of the canonical CaMK cascade were also present within IB4+ axons. CaMKIV is activated when phosphorylated by upstream CaMK kinases CaMKK1 and CaMKK2 (Wayman et al., 2008). Using an antibody that detects both CaMKK1 and 2, we observed punctate staining throughout confocal Z-slices of DRG, with a clear concentration of signal within IB4 positive axons (Figure 7A–C).

Expression of CaMK4 transcript variants in IB4+ neurons

The subcellular distribution of proteins is influenced by numerous mechanisms ranging from alternate splicing or alternate transcription start and termination sites to protein-protein interactions and post-translational modifications. Nuclear localization of CaMKIV is facilitated by its interaction with importin-alpha (Kotera et al., 2005) and requires the kinase to be catalytically active (Lemrow et al., 2004). However, it is currently unknown how axonal localization of CaMKIV is regulated. Given that axonal CaMKIV is predominantly expressed in the IB4+ population of DRG neurons and much less so in IB4- neurons, this provided us with an ideal system to attempt to elucidate possible regulatory mechanisms. We therefore examined the expression of known transcript variants in IB4+ neurons that highly express non-nuclear CaMKIV. In the rat, the *CaMK4* gene is expressed as 2 protein variants - the canonical protein CaMKIV-A (gene/mRNA *CaMK4*-A) and CaMKIV-B (gene/mRNA *CaMK4*-B), which comprises all of the CaMKIV-A protein with an additional short peptide sequence present on the N-terminus (Sun et al., 1995). This N-terminal peptide extension is encoded by an alternative 5' exon and start codon but there is no known function for this isoform. In total, there are 4 mRNA variants deposited in Genbank that differ at their 5' sequence (Figure 8Ai,ii): *CaMK4*-B is sequence S65840, *CaMK4*-A is M63334 and two additional variants of the *CaMK4*-A canonical sequence with alternate 5'UTRs, BC128706 and M64757 (Bland, 1993). There are no known functions for these different 5'UTRs. In addition to these previously described 5' isoforms, we also observed a conserved region of genomic DNA immediately downstream of and adjacent to the known termination site and running approximately 10kb in contiguous sequence (Figure 8Ai,iii).

Within this region there are clusters of expressed sequence tags (ESTs) running almost throughout its length prompting us to theorize that this sequence may be expressed, possibly as an extended transcript of *CaMK4*. EST data from other species mapping to this homologous region also support this proposition. For example, the mouse sequence curated by RefSeq includes this region as part of the *CaMK4* gene (mouse NCBI Reference Sequence: NM_009793.3).

To determine if IB4+ DRG neurons differentially express *CaMK4* transcripts with alternate 3' sequence variants, DRG from naïve rats were dissociated, stained with IB4 and sorted into IB4+/− cells using FACS (Figure 8B). The relative expression in IB4+/− cells of *CaMK4*-B (S65840) and of the two *CaMK4*-A variants (M64757 and BC128706) was determined by quantitative PCR (qPCR). These variants were expressed at approximately 10% the level of *CaMK4*-A, (sequence M63334), and expressed equally between IB4 positive and negative cell populations (Figure 8Ci). Expression of the putative 3' variant was determined using a qPCR probe mapping to the central EST cluster approximately 4.5kb downstream from the stop codon. We determined that this variant is expressed to a significantly higher level in IB4+ neurons than in IB4-negative (≈4-fold), and is expressed at 80% of the level of the coding region probed at the last exon boundary (Figure 8Cii). Genomic DNA contamination was not detected using qPCR templates prepared without reverse transcriptase (not shown).

To validate the expression of this novel transcript in DRG, two fluorescent *in situ* riboprobes were designed and synthesized, the first to specifically target the novel 3' region and the second to target the known CDS. Qualitative analysis of *in situ* hybridisation strongly indicated that although the CDS-targeted probe bound to essentially all neurons, the 3' probe bound to small and medium diameter neurons in a pattern very similar to that of IB4 (Figure 9A–F).

Characterisation of a 3'UTR-extended transcript of CaMK4

Sequence analyses of the novel 3' region expressed in IB4+ neurons did not predict the presence of any peptide-encoding open reading frames or splice sites. This, in addition to our observation of only a single clear band on Western blots of DRG-derived protein extracts, lead us to propose that the novel 3' region might be an extended 3'-UTR variant involved in regulation.

3'UTR's contribute to cell-type specific or developmental-stage specific regulation of gene functions by modifying cellular localization, stability and/or translational efficiency of transcripts (for review see Neilson and Sandberg, (2010)). Varying 3'UTR lengths can be generated by alternate polyadenylation, allowing mRNA elements downstream of the stop codon to be included or excluded, or by alternate splicing. Differential 3'UTR sequences can include miRNA consensus binding sites or RNA-binding protein motifs that perform a multitude of functions. To determine if differential polyadenylation might account for the RNA expression data described above, the polyadenylation site prediction algorithm POLYAR was used to test for putative tandem 3' polyadenylation signals downstream of the *CaMK4* stop codon (Akhtar et al., 2010). POLYAR takes into account the position of the cleavage site (CS) relative to the upstream polyadenylation signal (PAS) and the U-/GU-rich down steam element (DSE). POLYAR then generates a score (W) for each putative site, with higher scores indicating cleavage sites closer to the ideal. The canonical PAS at 2375 nucleotides downstream of the start codon gave a W score of 45.64. POLYAR analysis predicted 7 other putative sites with W scores above 45 (Figure 10A). They split into two further clusters of tandem sites: The first 5535, 5914 and 6348 nucleotides downstream and the second cluster 8183, 10074, 10904 and 11801 nucleotides downstream of the start codon.

We next sought to validate the *in silico* predicted sites using 3' rapid amplification of cDNA ends (3'RACE) (Borson et al., *1*992). Specific primers were designed to lie between 200 and 900 bp upstream of each predicted site, generating 7 sets of primers for RACE reactions (RACE_A through RACE_G). Note that the RACE_C reaction was used for both sites #3 and #5 because they lie within 400bp of each other. 12 bands from all reactions were obtained for sequencing, 2 of which positively mapped to the *CaMK4* gene. These validated polyA cleavage sites included the canonical site (#8, RACE_G) and a novel as yet undescribed site 11801bp downstream of the *CaMK4* start codon (#1, RACE_A) (Figure 10B, D).

We next sought to determine if the predicted alternate polyadenylation site was transcribed in continuity with the coding sequence of *CaMK4* in adult rat DRG mRNA. To achieve this we employed sequence-specific primers in the reverse transcriptase-catalyzed synthesis of cDNA. Following synthesis of cDNA generated specifically by a primer targeting the putative 3' extension, PCR was performed using tandem contiguous 800bp probes mapping from the *CaMK4* start codon, through the coding region and the length of the putative 3' extension. PCR reactions with template generated from cDNA reactions without primer were used as a negative control (Figure 10C, lane labeled -p). Positive PCR signals were detected when the 3'-targeting primer was used to generate cDNA (Representative reaction: Figure 10C, lane labeled gene specific primer - GSP), demonstrating that the novel 3' region was contiguous with the coding region of *CaMK4*.

To determine the exon structure of this novel transcript, all PCR products were then sequenced, the contiguous products (contigs) assembled and the resulting sequence aligned to the rat genomic sequence. This sequence aligned with 100% homology to all exons from the start codon, including the stop codon, through the annotated 3'UTR a further 4000 nucleotides downstream and terminating at the GSP probe position. Thus, all protein coding elements including the stop codon are present. When considered with our finding that there were no higher molecular weight bands detected on Western blots (Figure 1), these data indicate that the novel transcript described here is a 3'UTR variant of *CaMK4* most likely generated by alternate polyadenylation (APA) at tandem (cis) sites.

Characterisation of RNA-Binding Protein Sites within the CaMK4 3'UTR

3'UTR extension is proposed as a mechanism for regulating the stability of mRNA and/or sub-cellular location of transcripts for local translation. This is often driven by association of the UTR with RNA-binding proteins (RBPs). We therefore analysed the novel 3'UTR to determine predicted RBP sites using position weight matrices (PWMs) from the RNA binding protein databank (RBPDB). Predicted binding sites were determined for rat, mouse and human. RNA binding proteins with two or more predicted binding sites in either of these species are shown (Table 6).

Interaction with the Embryonic Lethal Abnormal Vision (ELAV)/Hu family of RNAbps regulates mRNA stability. We therefore sought to determine whether ELAVL1 (HuR) might bind to the novel *CaMK4* 3'UTR by analysing publically available RNA immunoprecipitation-high-throughput sequencing (RIP-Seq) data (Figure 11). RIP-Seq involves immunoprecipitation of RNA-protein complexes and therefore serves to validate the predicted binding. Conserved ELAVL1 binding sites were uncovered by determining the intersection between rat/mouse/human homologous regions (Figure 11Aii) with the RIP-seq peaks (Figure 11Aiv). This analysis indicated that ELAVL1 binding is increased as the UTR is extended.

In order to determine if this relationship was specific to the *CaMK4* 3'UTR, or a function of UTRs in general, we compared the number of ELAVL1 binding sites within the novel

CaMK4 3'UTR with those of 3'UTRs of other genes. The number of ELAVL1 binding sites within the 3'UTR of 2000 random Ensembl transcripts was compared to the number in *CaMK4* (Figure 11B). UTRs of most of the randomly-selected transcripts contained no ELAVL1binding sites (~1800). While those predicted to bind ELAVL1 contained a variable number of sites only 2% had a greater number of ELAVL1 binding sites (normalized by transcript length) than for *CaMK4*, while 98% had significantly fewer binding sites than *CaMK4*.

Discussion

In this study we examined the expression of CaMKIV protein in sensory neuron somata in DRG and its distribution in axons of the spinal nerve of the adult rat. Given that this determination required an immunohistochemical approach we obtained a number of commercially available antibodies and assessed their specificity. This was especially required given the well-described role of CaMKIV in the nucleus of cells/neurons where it regulates transcription. Although it has long been recognized that CaMKIV is also present outside the nucleus where it is activated by upstream signals, not all CaMKIV-expressing neurons display notable non-nuclear signal and no function has yet been ascribed to its location in axons. The homologous family member CaMKI, similar both in terms of sequence and in function, is known to have an axonal/dendritic role and so it was imperative to rule out any cross-reaction of antisera with this and other CaMK family members. These assessments validated two different antisera raised in different species against largely distinct regions of CaMKIV, both recognizing similar bands on Western blots with little observed non-specific interactions and both giving highly similar immunological stains, thus demonstrating the utility of these reagents to characterise the distribution of CaMKIV.

CaMKIV subcellular distribution differs based on sensory neuron type

Given previous observations of limited co-staining with CGRP (Ji et al., 1996), we performed triple labeling experiments to determine the expression levels of CaMKIV in relation to the population markers IB4 and CGRP. We observed, as did the previous study, that CaMKIV expression is greater in smaller diameter neurons than larger diameter, and that only a subpopulation of CGRP+ cells contains elevated CaMKIV. Conversely, IB4 staining is a highly predictive marker for CaMKIV expression. This does not contradict prior studies as many neurons display both IB4-binding and CGRP-expression in rat (Wang et al., 1994). Indeed, the Ji et al. (1996) study concluded that the majority of the highest intensity CaMKIV expression (which would include those we classify as expressing non-nuclear CaMKIV) did not express CGRP Thus, it appears that essentially all sensory neurons of the DRG express CaMKIV in the nucleus, but that a subset expresses CaMKIV which becomes elevated outside the nucleus. The subpopulation with elevated CaMKIV is almost entirely encompassed within the IB4-binding population, with CGRP-expression relating to non-nuclear CaMKIV expression principally (though not entirely) based on the overlap of CGRP and IB4. Conversely, essentially all IB4-binding neurons display elevated non-nuclear CaMKIV.

CaMKIV has previously been observed distal to the cell body in sciatic nerve (Ji et al., 1996). Using high magnification confocal imaging and co-localisation analyses we have demonstrated that CaMKIV is concentrated within IB4-binding axons in spinal nerve. However, approximately 30% of this protein is detected outside of these axons suggesting that it plays a role in other axons or other cells in nerve tissue. For example, it is possible that CaMKIV is expressed in Schwann cells, which also express members of the CaMK cascade including CREB (e.g,: Stewart 1995).

Possible mechanisms regulating the location of CaMKIV to axons

A diverse array of mechanisms exists to regulate the extent a given protein is targeted to sub-cellular domains. Such mechanisms include regulation of protein-protein interactions by various means, changes in the extent of post-translational modification such as glycosylation and alternate splicing of exons containing targeting sequences. Protein targeting is regulated by linear amino-acid motif signal sequences or by cryptic signal patches that form part of larger protein domains. These signals may be included or excluded by differential splicing (e.g., Poëa-Guyon et al., 2006), conferring differential sorting from the trans-Golgi network to axons or otherwise (Lasiecka and Winckler, 2011). We therefore sought to determine if the IB4-binding neuron population expressed CaMKIV-β which contains an N-terminal extension coded by an alternate exon at the 5' end of the gene. This CaMKIV protein variant is expressed in specific neurons including cerebellar granule neurons suggesting that it is functional, but this function remains unclear (Sakagami et al., 1999). qPCR analysis of known *CaMK4* transcript variants in FACS-sorted IB4+ neurons showed that 5' variants including *CaMK4*-β, are expressed to a low level in all DRG cells regardless of IB4-biding status. Of note, the analysed 5'UTR variants include sequence BC128706 which is the Genbank consensus rat mRNA, however the 5'-most exon of this sequence is expressed at a low level in DRG. Together these results make it very unlikely that the documented variation at the 5' end of the gene, both coding and non-coding, is involved in axonal targeting in DRG neurons.

At the level of mRNA, transcript variants can introduce motifs for RNA-protein binding and/or influence the stability of RNA and therefore local concentrations of protein and/or influence transport of the mRNA to the required compartment for local translation. At the 3' end of the gene, there is a series of ESTs in Genbank, which are moderately conserved between vertebrate species. We hypothesised that this could be a signature of multiple 3'UTR-extended forms of rat *CaMK4*. In addition, an extended 3' form is present in the mouse refseq (NM_009793.3) but to the best of our knowledge has not been formally described. Using RACE in tandem with DNA sequencing of the obtained PCR products we observed that *CaMK4* message can be extended past the canonical transcription termination site a further 10kb downstream to a novel and highly conserved alternate site including the core CS and putative auxiliary upstream URE and downstream DSE elements indicated by sequence homology. It should be noted that this extended transcript may have previously been observed using northern blot analysis of brain total RNA in a prior study (Bland et al., 1994). In this paper, the authors briefly mention a robust unexpected 10kb+ band in addition to the predicted *CaMK4* transcript of approximately 3kb.

Using reverse transcription primed with a gene specific primer mapping to the novel UTR, we have demonstrated that this sequence is contiguous with the *CaMK4* CDS including the catalytic domain. We do not have reason to believe that the adjoined RNA leads to a change in CaMKIV amino acid composition because the stop codon remains within this transcript and we do not see any higher molecular weight bands using Western blotting analysis. We validated the expression of this UTR in DRG tissue sections using *in situ* hybridization with 2 probes, one designed to recognize the UTR alone or another probe mapping to the CDS that detects all CDS-containing *CaMK4* transcripts. *CaMK4* message was detected in seemingly all neurons whereas the 3'UTR-extended form only in smaller neurons. We believe that these “UTR+” neurons determined by *in situ* fluorescence are likely to be the IB4+ population. qPCR quantification of the UTR in FACS sorted IB4+ cells showed that 80% of CaMKIV transcripts in IB4+ neurons have the extended 3'UTR. This situation can be accounted for if 1) 20% of CaMKIV transcripts are terminated prior to the qPCR probe or 2) 20% of IB4+ neurons do not express the UTR, or a combination of these. Neurons lacking IB4-binding express 4-fold less of this transcript than do IB4+ cells, correlating with

axonal localisation of protein. However, 20% of transcripts in this pool do contain the UTR suggesting that either, 1) IB4+ neurons express 4-fold less UTR-containing transcripts or 2) it is possible that the UTR is expressed in non-neuronal IB4− cells present in the FACS sort. However, this determination requires fluorescence *in situ* hybridization studies co-staining with IB4 and including cell counts and intensity assessments.

Given the inherent tendency of RACE to give false positive PCR products in addition to being insensitive to some 3' ends, the possibility still remains that other 3'UTR variants with alternate polyA (APA) sites exist, yielding UTRs of different lengths to the one we observed. The POLYAR computational analysis predicted multiple polyA sites but is also prone to type 1/2 errors. Also, POLYAR was directed to return only canonical PAS sites containing upstream and downstream elements with strong sequence homology. Many mRNAs do not have these and so would be missed by this computational prediction. Regardless, the EST data fall into clusters along the length of the UTR strongly suggesting that other non-characterised APA sites do indeed exist.

Axonal targeting of proteins is thought to be regulated by multiple mechanisms at multiple levels. Yet, through our observations that the 3'UTR-extension is highly and selectively associated with the cells that have axonal CaMKIV and that we see no such variation in protein coding sequences, we propose that tandem APA is a mechanism for differentially regulating axonal-targeting of CaMKIV. Mechanisms of tandem polyA site selection include differential recruitment of core 3' processing proteins (e.g., cleavage stimulation factor, CstF), RNA-binding proteins and transcription factors and auxiliary sequences (e.g,. U/GU-rich DSEs), RNA structure and chromatin status (Di Giammartino et al., 2011). APA sites can lie contiguously on the last exon, termed tandem APAs, or can occur by alternate splicing of 3' exons. Depending on species, around 50% of vertebrate genes have alternative polyadenylation sites, and approximately 50% of those sites are generated from tandem PAS sites within the same exon rather than in alternate exons (Tian et al., 2005). The APA we have characterised lies on the same exon, extended 10kb downstream as determined by sequence analysis of contiguous cDNA PCR fragments. The novel 3'UTR of *CaMK4* characterised in this study is long (10kb) but certainly not of an unusual length. For example, the well characterised UTR of Methyl-CpG-binding protein 2 gene (MeCP2) is around 8.5kb (Newnham et al., 2010). Bioinformatic estimates of the number of genes that may have UTRs in the range of 5–10kb in length are in the order of 5000 human genes (Lopez et al., 2006) at least 80 of which have been experimentally validated using PCR techniques (Moucadel et al., 2007).

UTRs most often function at least in part to regulate the stability of mRNAs. Regulation of protein synthesis can be attenuated by miRNAs which bind to 3'UTRs and target them to the RISC complex for degradation. Extension of the 3'UTR of *CaMK4* introduces a number of predicted miRNA sites (unpublished data). It is worth noting, though, that in rare cases, miRNAs can have a positive effect on translation (Ghosh et al., 2008). mRNA stabilisation resulting in increased protein synthesis rates is regulated by interactions with RNA binding proteins. Our bioinformatic analyses using consensus motif position weight matrices (PWMs) predict that a number of RNA binding protein binding sites are introduced by *CaMK4* 3'UTR extension. Many of these could influence *CaMK4* RNA stability, but we concentrated our analyses and discussion on the Embryonic Lethal Abnormal Vision (ELAV)/Hu family proteins owing to the availability of experimentally validated high-throughput RNA-binding data (Dunham et al., 2012).

The importance of 3'UTR sequences for regulating RNA stability has been known for some time. For example AU-rich elements (AREs) present in UTRs and discovered in 1986 (Shaw and Kamen, 1986), have a mostly negative effect on stability (Chen and Shyu, 1995).

However, this destabilizing effect of AU elements is blocked by interaction with ELAV1 (HuR) (Peng et al., 1998). In addition to this, ELAV1 can stabilize RNA by repression of miRNA binding (Meisner and Filipowicz, 2011). Using publically available high throughput data we were able to demonstrate that ELAVL1 binds to the 3'UTR of *CaMK4* at multiple highly conserved sites, strongly suggesting that there is a functional implication for this interaction. We therefore postulate that extension of the *CaMK4* 3'UTR would result in the introduction of destabilizing AU motifs and as a result, the continued stability of *CaMK4* message within IB4+ neurons would require an available pool of AU-blocking ELAVL1 protein. This interplay between AU-containing UTR elements and ELAVL1 protein could then establish an efficient mechanism to regulate axonal levels of *CaMK4*.

ELAVL2 (HuB) is predicted to bind the *CaMK4* UTR at multiple sites (Table 6). This protein is expressed to a high level in DRG (Okano and Darnell, 1997) although its expression in subpopulations within the DRG is undocumented. HITS-CLIP analysis has shown that ELAVL2 binding is enriched in genes regulating neuronal projection (Ince-Dunn et al., 2012), perhaps suggesting that interaction with *CaMK4* may have a similar role. Through interaction with AU and/or GU elements, there is also accumulating evidence that ELAV-RNA interactions play an important role in neuronal development and plasticity by 1) targeting mRNA to subcellular compartments though interactions with microtubules (Fujiwara et al., 2011), 2) though interaction with RNA and ribosomes in growth cones (Pascale et al., 2008) and 3) dendrites (Bolognani et al., 2004) and by 4) stabilizing growth associated genes (Pascale et al., 2004).

Given that UTR extension often decreases the stability of mRNA, then any potential destabilization must be counteracted in IB4+ neurons that express elevated levels of both extended transcript and protein. This stabilisation of the extended transcript may take place through interaction with RNA-binding proteins such as ELAVL1 that may block miRNA targeting and/or AU-element driven degradation, thus forming a dynamic mechanism for regulating *CaMK4* mRNA abundance. Increased mRNA stability amounts to increased protein production and this may increase sorting through and axonal targeting from the trans-golgi network.

Finally, a tantalising possibility exists that the 3'UTR encodes elements for distribution of mRNA to axons for local translation. mRNA is transported to sub-cellular locale in response to a variety of signals (Willis et al., 2007) to dendrites (Mayford et al., 1996) and also to axons (Willis et al., 2011) *in vivo*. mRNA is transported by association with RNA-binding proteins (RBPs) that interact with motifs within UTRs and package transcripts into transport granules (Rossoll et al., 2003). Using a computational approach we have uncovered putative *CaMK4* 3'UTR RBPs. A number of these may influence *CaMK4* RNA location to axons, for example hnRNPA1 and hnRNPK, members of the heterogeneous nuclear ribonucleoprotein (hnRNP) family that plays an important role in mRNA transport in axons (Rossoll et al., 2003; Raju et al., 2008; Glinka et al., 2010).

Possible Roles of Axonal CaMKIV in IB4 neurons

At present, it is not clear what the presence of CaMKIV in axons indicates about its function or role. In our analyses, non-nuclear CaMKIV expression correlated very strongly with IB4 binding. Thus, it serves to consider the known roles of CaMKIV in conjunction with the known characteristics of IB4+ neurons that set this group apart from other DRG neurons in the intact adult animal. In contrast, it also serves to consider our observations alongside the known roles of CaMKIV in these and other sets of neurons. It may then be possible to generate a working hypothesis of the convergent function of axonal CaMKIV.

The following discussion examines 1) general characteristics of IB4-binding DRG neurons, 2) the mechanistic roles of CaMKIV in signal transduction pathways, and then considers possible functions for this protein in 3) plasticity and 4) nociception and pain.

1) Characteristics of IB4-binding DRG neurons—The IB4-binding population of DRG neurons gives rise to unmyelinated axons (Streit et al., 1985; Wang et al., 1998a), and displays properties consistent with nociceptive functions (e.g., (Petruska et al., 2000a; Petruska et al., 2000b; Fang et al., 2006). IB4-binding DRG neurons predominantly innervate cutaneous targets, but also provide more limited innervation of visceral tissues (particularly hollow organs such as bladder and colon) and muscle targets, and to a much lesser degree joint and vertebral disc (Aoki et al., 2004, 2005; Bennett et al., 1996; Fundin et al., 1997; Ivanavicius et al., 2004; Kitao et al., 2002; Kuniyoshi et al., 2007; Nakajima et al., 2008; Petruska et al., 1997; Ramarli et al., 1986; Rau et al., 2007; Wang et al., 1998 b; a). It is important to note also that the proportion of cutaneous and non-cutaneous IB4-binding DRG neurons is likely to vary by segment, as each DRG innervates a different complement of tissues.

IB4-binding DRG neurons thus appear to innervate predominantly tissues with epithelium. Of course, the type of tissue innervated does not necessarily indicate why these neurons rather uniquely express non-nuclear CaMKIV, nor does it indicate what sort of role the non-nuclear CaMKIV is playing – certainly non-IB4-binding C-fiber neurons (which according to our data have little/no axonal CaMKIV) innervate the same tissues, including epithelium. Nonetheless, epidermis, the major target of IB4-binding axons (Fundin et al., 1997; Ramarli et al., 1986; Rice 1993), is notable for its high rate of turnover. Presumably this requires that the terminal arbors embedded in it display a high degree of constitutive local plasticity capacity. Epithelial turnover is governed to a large part by a calcium gradient that exists through the entire depth of the tissue layer (Bikle et al., 2012), providing one way in which CaMKIV may play a local role in maintaining axonal structure within a constantly remodeling tissue. A final consideration is that the epithelial innervation appears to differ according to IB4-binding, with the axons that are most interwoven among epidermal cells, and extend most superficially being those that bind IB4 (defined directly or as being nonpeptidergic), while those lacking IB4-binding do not extend as far and have relatively straight projections (e.g., Fundin et al., 1997; Rice 1993; Zylka et al., 2005).

2) Signal Transduction—Our analyses indicate that approximately 20% of CaMKIV in any given IB4+ axon is associated with the signaling endosome marker Rab7 indicating that at least a proportion of CaMKIV in each IB4+ axon could be involved in endosome-mediated signaling. Rab7 plays a well-defined role in retrograde signaling from the tyrosine kinase receptors (Trks) – TrkA, TrkB and the low affinity receptor p75 – where Rab7-decorated endosomes are associated with increased cell survival and/or neurite outgrowth (Saxena et al., 2005; Deinhardt et al., 2006). In addition, the receptor tyrosine kinase RET, associated with Glial Cell-Derived Neurotrophic (GDNF) Receptors (GFRs) and expressed by IB4+ sensory neurons (Molliver et al., 1997; Bennett et al., 1998), is internalized and sorted into Rab5 endosomes (Richardson et al., 2006). Rab5 early endosomes are sorted into Rab7 signaling endosomes for axonal transport in DRG axons (Deinhardt et al., 2006), suggesting that GDNF:RET signaling could also be transmitted in Rab7 endosomes, however this has not yet been established. In our analyses, all IB4+ axons appeared to contain CaMKIV, but very few IB4-negative axons showed CaMKIV immunoreactivity. A proportion but not all of IB4+ neurons also express TrkA, and a large proportion of TrkA+ neurons are not IB4-binding (Verge et al., 1989; Wang et al., 1994; Molliver et al., 1997). Therefore, it is very likely that many of the NGF-sensitive neurons do not express axonal CaMKIV. Also, the small-diameter neurons that express GRF-alpha and RET are nearly all IB4-binding, and are therefore sensitive to GDNF ligands (Molliver et al., 1997; Bennett et

al., 1998; Gavazzi et al., 1999; Leitner et al., 1999), and so it is possible that axonal CaMKIV acts downstream of GDNF signaling.

It is established that CaMKIV is phosphorylated and activated by CaMKK1/2 in the cytoplasm in response to cytoplasmic calcium signaling, and this modification is required for its entry into the nucleus (Lemrow et al., 2004). We have shown that CAMKK is present in IB4+ cytoplasm and also in IB4+ axons in peripheral nerve, thus placing it in a position where it could possibly activate CaMKIV outside the soma. An analogous situation exists for the closely related family member CAMKI. Like CaMKIV, CAMKI responds to intracellular calcium and is activated by CAMKK. CAMKI is a positive regulator of neural plasticity during activity dependent synaptogenesis (Saneyoshi et al., 2008) and axon/dendrite growth (Wayman et al., 2004, 2006) where the CAMKI-alpha isoform is responsible for dendritic and the CAMKI-γ isoform is responsible for axonal functions (Neal et al., 2010). Therefore CaMKIV and CAMKI may share a functional overlap when co-expressed in axons. However, known differences in their substrate affinities (Corcoran et al., 2003) suggest that these 2 kinases should be considered independently despite their similar functions and close homology. Interestingly, upon stimulation of Neuro-2a cells with ionomycin, CaMKIV but not CAMKI, phosphorylates LIM kinase I (LIMK1) (Takemura et al., 2009). This modification of LIMK1, which activates cofilin to regulate actin dynamics, is critical for neurite extension. Further, although CAMKI also has a positive effect on neurite outgrowth, this does not occur though the LIMK-cofilin pathway. Given our observations, it is possible that this pathway is activated by CaMKIV in sensory neuron fibres, suggesting a role for CaMKIV in this compartment that is distinct to that of CAMKI. Additional considerations on this are provided below (role in plasticity).

A characteristic of growth factor signals is that they occur in distinct units that function to localise the ongoing signal cascade. These units include lipid rafts at the cell membrane and within endosomes (Hoeller et al., 2005). Endosomes contain both the catalytically active receptor and their specific effectors in close proximity. Therefore, the presence of CaMKIV in endosomal compartments may allow it to preferentially access these effectors. To exert a transcriptional effect axonally-derived signals must be conveyed to the cell body. Upon entering the cell body, this signal must be distinguished from signals that originate within the soma. This distinction can be achieved by specific proteins that decorate endosomes. We have observed that a proportion of CaMKIV is associated with Rab7 decorated endosomes. As far as we are aware, this is the first demonstration of any CAMK family members localized within Rab7 endosomes. Our observations suggest that the canonical CAMK pathway including upstream activating kinases (CAMKK-I and -II) could activate CaMKIV within the axons of IB4-binding neurons prior to transport in endosomes for activity (transcription/splicing) within the nucleus.

The role of, and transport mechanism for, the non-Rab7-associated IB4-axonal CaMKIV (approx. 80% of axonal CaMKIV) is unclear. There is precedent for selective retrograde transport of locally activated proteins as is the case for ERK 1/2 (Perlson et al., 2005) and STAT3a (Ben-Yaakov et al., 2012) and for selection into Rab7 positive (intermediate-speed carriers) or Rab7 negative (fast-speed carriers) (Deinhardt et al., 2006) endosomes. Also, in addition to endosomal transport, retrograde traffic may be achieved by direct interaction with nuclear importins (Hanz et al., 2003). This possibility is especially attractive because CaMKIV is known to interact with importin-alpha and this is required for nuclear entry. Also, using nerve ligation experiments *Ji* et al. (1996) observed that CaMKIV concentrated on both sides of the ligature suggesting that a proportion of the axonal CaMKIV we observe is anterogradely transported. By observing the association of CaMKIV with other markers of specific transport modes, it may be possible to tease apart any divergent signaling modes involving CaMKIV within populations of axons.

The occurrence and activity of CaMKIV outside of the nucleus is not unprecedented. Proposed roles for extranuclear CaMKIV activity include the regulation of microtubule dynamics by phosphorylation of the microtubule binding protein stathmin (Melander Gradin et al., 1997). Stathmin is activated upon stimulation with NGF and regulates neuronal polarity and axonal growth (Di Paolo et al., 1996). Also, CaMKIV phosphorylates the Ras-related GTP-binding protein (Sahyoun et al., 1991) Rap1b which is associated with endosomes (Pizon et al., 1994). It remains to be determined if these activities are relevant for IB4+ neurons.

It must also be considered that while the majority of our analyses and discussion center on IB4+ axonal CaMKIV, nearly all IB4− DRG neurons express CaMKIV to some degree where it appears concentrated in nuclei. Thus, CaMKIV per se may be involved with many more processes than we have considered here. Further, subcellular distribution of CaMKIV could change based on conditions, meaning that neurons that express mostly nuclear-localized protein in one condition could upregulate axonally transported protein in another condition, and vice-versa. Given the demonstrated importance of CaMKIV in neurons, determining the regulation of its subcellular distribution should prove a very fruitful line of investigation.

3) Neural Plasticity—CaMKIV is well-known to support diverse subsets of plasticity modes that are contingent on specific input paradigms. CaMKIV KO mice are deficient in cerebellar and hippocampal long term potentiation (LTP) (Ho et al., 2000). However, germline over-expression of dominant-negative CaMKIV (dnCaMKIV) restricted to the forebrain of mice impairs L-LTP in the hippocampus and affects long term memory with no significant effect on the early phase of LTP (Kang et al., 2001). Also, in CaMKIV KO mice the maintenance of cerebellar LTD is abolished where motor memories for increases in gain of the vestibulo-ocular reflex are impaired, whereas memories for decreases in gain are unaffected (Boyden et al., 2006), indicating the specificity of the role of CaMKIV in plasticity. Acute over-expression of constitutively active CaMKIV in adult rat hippocampus enhances NMDA receptor-mediated synaptic responses in addition to LTP (Marie et al., 2005). Interestingly, this is concomitant with the formation of excess silent synapses which may later effect the consolidation of plasticity.

Multiple reports have demonstrated that CaMKIV has a positive effect on neurite outgrowth *in vitro*, though others have found no effect (Hansen et al., 2003). In embryonic cortical cultures and slices, calcium induced dendritic growth is regulated by CaMKIV-mediated CREB activation (Redmond et al., 2002), similar to what others have reported in cultured hippocampal neurons and Neuro 2a cells (Tai et al., 2008; Takemura et al., 2009). Importantly, in cortical neurons that heterogeneously express differing amounts of native CaMKIV, dendrite complexity increased in direct association with increased levels of the protein (Nagendran and Hardy, 2011). siRNA mediated reduction of the endogenous protein then reduces branching and elongation of dendrites both under basal conditions and during activity-induced elaboration. This latter study is particularly compelling as its conclusions arise out of manipulating the endogenous protein, unlike many other studies which have relied on over-expression plasmids for gain and loss of function experiments where dominant negative CaMKIV (dnCaMKIV) inhibits and constitutively active CaMKIV (caCaMKIV) enhances growth. However, the effects of dn/caCaMKIV are not clear-cut and inconsistencies exist in the literature. For example Wayman et al. (2004) demonstrated that dnCaMKIV inhibited axon growth when using a plasmid lacking a nuclear localization sequence (NLS), but did not affect axon growth when the plasmid included a NLS (Wayman et al., 2004). They reasoned that dnCaMKIV, being unable to locate to the nucleus, artifactually sequesters CAMKK in the cytoplasm thereby blocking its activation of substrates required for outgrowth, which likely includes CAMKI. In support of this, they

argued that the constitutively active mutant of CaMKIV had an artifactually positive effect by mimicking the role of CAMKI. It is broadly, though importantly not entirely, maintained that CAMKI is the extra-nuclear regulator of CAMK family-mediated neurite outgrowth and that the role of CaMKIV lies exclusively in the nucleus and does not regulate axon growth (Wayman et al., 2011). However, Kamata et al., (2007) observed a significant reduction in cultured hippocampal dendrite length after transfecting a dnCaMKIV mutant including an NLS and the reason for this discrepancy remains unclear (Kamata et al., 2007). Over-expression of caCaMKIV does not necessarily increase rates of neurite growth. For example, a concomitant increase in levels of cAMP suppresses this effect (Spencer et al., 2008), suggesting that there may be a ceiling to outgrowth as assessed in that mode. Interestingly, virus-delivered caCaMKIV enables cerebellar granule neurons (CGNs) to overcome the inhibitory influence of myelin-associated glycoprotein (MAG) on neurite extension (Spencer et al., 2008). Together, these studies largely suggest that CaMKIV plays a positive role by disinhibiting neurite outgrowth and arbor complexity under conditions where these processes are limited.

DRG neurons, particularly those with unmyelinated axons, are certainly capable of significant structural plasticity (e.g., Diamond et al., *1*992). However, the above studies of CaMKIV function have mainly focused on dendritic plasticity and DRG neurons are believed to not possess dendrites, at least by most definitions. It is interesting to consider that, in terms of the transduction of electrophysiological signals and in the collection of information, sensory terminals in the periphery are indeed akin to the dendrites of CNS neurons. This is particularly true of the terminals of C-fiber neurons which are very large highly-branched structures that are not associated with specialized end-organs – perhaps their highly-plastic terminal structure is maintained by molecular mechanism shared with dendrites.

4) Nociception and Pain—Non-nuclear CaMKIV is enriched in IB4-binding small diameter sensory neurons. The majority of these neurons are nociceptors – neurons transducing actually or potentially tissue damaging stimuli (Petruska et al., 2000b, 2002; Fang et al., 2006) – which raises the question of a possible role for axonal CaMKIV in nociception. Nociceptors have a variety of mechanisms that confer sensitivity/responsiveness to Ca^{2+}, including Ca^{2+}-permeable stimulus transduction channels (e.g., TRP family) and voltage-gated ion channels that pass Ca^{2+} with each action potential. It is possible that axonal CaMKIV may be involved in some of the constitutive stimulus-transduction and/or signal-transmission processes that may be unique to IB4-binding DRG neurons in the naïve condition. Given the role in other neurons of CaMKIV in plasticity and adaptive processes reliant on activity and/or calcium influx, it is possible that CaMKIV may emerge as playing a role in plasticity processes such as the sensitization/desensitization response and/or axonal terminal growth processes known for nociceptors, irrespective of any role it may have in basal functioning. In rat, IB4-binding neurons include those displaying strong responses to capsaicin (e.g., Petruska et al., 2000b), often considered a chemical surrogate of noxious heat, via activation of the TRPV1 channel which has high calcium permeability (e.g., Oh et al., 1996). It is compelling to note that the known Ca^{2+-} dependent desensitization of TRPV1 is strongly dependent on Ca^{2+}/calmodulin (Rosenbaum et al., 2004), and that TRPV1 desensitization and responsiveness can be modulated by trophic factors (e.g., Shu and Mendell, 2001; Galoyan et al., 2003; Amaya et al., 2004; Malin et al., 2006).

Summary

We have determined that high levels of CaMKIV protein are expressed by IB4-binding sensory neurons of the DRG, and that this protein is localized outside of the nucleus in the

axon. The mechanisms regulating, and the functional implications of this unique subcellular localization are currently unclear. Given the importance of CaMKIV in other neurons/cells and contexts, these topics should prove to be fruitful areas of investigation. We have begun this process through experimental identification of at least one mechanism which could regulate the subcellular localization. We have determined that the IB4-binding neurons express comparatively high levels of a novel 3'-UTR-extended variant of CaMKIV mRNA, which could provide the means for differential sub-cellular protein targeting. Using computational analyses of binding sites in addition to published RNA-protein interaction data we have also determined that this 3'-UTR-extended interacts with ELAVL/hu proteins, RNA binding proteins which have been shown to affect subcellular localization in other contexts. Also, by considering the convergence of known functions of CaMKIV and the known and suggested functions of IB4-binding sensory neurons, we suggest roles this protein may be playing in IB4+ axons. It is exciting to consider that the emerging understanding of how mRNA variants influence protein function, a regulatory mechanism highly concentrated in the nervous system (e.g., Barry and Mattick, 2012; Mattick, 2011), may significantly advance our understanding of activity/calcium-mediated functions of sensory neurons.

Acknowledgments

We thank Kristofer K. Rau for histology support, Jason E. Beare for microscope and image analysis support, Darlene A Burke for statistics support, Chris Worth for technical assistance with FACS and Simon Halegua for helpful guidance with endosome markers.

Role of Authors All authors had full access to all the data in the study and take responsibility for the integrity of the data and the accuracy of the data analysis. Study concept and design: BJH, JCP. Acquisition of data: BJH, RMF, CG, GV. Analysis and interpretation of data: BJH, RMF, CG, GV, SRE, US, JLT, ECR, JCP. Drafting of the manuscript: BJH, RMF, JLT, JCP. Critical revision of the manuscript for important intellectual content: BJH, RMF, CG, SRE, US, JLT, JCP. Statistical analysis: BJH, RMF, JCP. Obtained funding: BJH, SRE, US, JLT, JCP. Administrative, technical, and material support: BJH, RMF, CG, GV, US, JLT, ECR, JCP. Study supervision: ECR, JLT, JCP.

GRANT INFORMATION: Paralyzed Veterans of America Fellowship (2579 to BJH). Kentucky Spinal Cord and Head Injury Research Trust (9–12A and 10–10 to JCP), NSF (MCB-1020970 to JLT), USAMRMC (W81XWH-10-2-0082-CLIN 1 to US), JGBCC-OCRP to US, NIH (R21NS080091 to JCP; 8P20GM103436-12 to ECR; P30GM103507 (PI – S.R. Whittemore) supporting the KSCIRC Core facilities).

Literature Cited

Ahn S, Ginty DD, Linden DJ. A Late Phase of Cerebellar Long-Term Depression Requires Activation of CaMKIV and CREB. Neuron. 1999; 23:559–568. [PubMed: 10433267]

Akhtar M, Bukhari S, Fazal Z, Qamar R, Shahmuradov I. POLYAR, a new computer program for prediction of poly(A) sites in human sequences. Bmc Genomics. 2010; 11:646. [PubMed: 21092114]

Amaya F, Shimosato G, Nagano M, Ueda M, Hashimoto S, Tanaka Y, Suzuki H, Tanaka M. NGF and GDNF differentially regulate TRPV1 expression that contributes to development of inflammatory thermal hyperalgesia. Eur J Neurosci. 2004; 20:2303–2310. [PubMed: 15525272]

Aoki Y, Ohtori S, Takahashi K, Ino H, Douya H, Ozawa T, Saito T, Moriya H. Expression and co-expression of VR1, CGRP, and IB4-binding glycoprotein in dorsal root ganglion neurons in rats: differences between the disc afferents and the cutaneous afferents. Spine. 2005; 30:1496–1500. [PubMed: 15990662]

Aoki Y, Takahashi Y, Ohtori S, Moriya H, Takahashi K. Distribution and immunocytochemical characterization of dorsal root ganglion neurons innervating the lumbar intervertebral disc in rats: a review. Life Sci. 2004; 74:2627–2642. [PubMed: 15041445]

Barry G, Mattick JS. The role of regulatory RNA in cognitive evolution. Trends Cogn Sci. 2012; 16:497–503. [PubMed: 22940578]

Bennett DL, Dmietrieva N, Priestley JV, Clary D, McMahon SB. trkA, CGRP and IB4 expression in retrogradely labelled cutaneous and visceral primary sensory neurones in the rat. Neurosci Lett. 1996; 206:33–36. [PubMed: 8848275]

Bennett DL, Michael GJ, Ramachandran N, Munson JB, Averill S, Yan Q, McMahon SB, Priestley JV. A distinct subgroup of small DRG cells express GDNF receptor components and GDNF is protective for these neurons after nerve injury. J Neurosci Off J Soc Neurosci. 1998; 18:3059–3072.

Bikle DD, Xie Z, Tu C-L. Calcium regulation of keratinocyte differentiation. Expert Rev Endocrinol Metab. 2012; 7:461–472. [PubMed: 23144648]

Bland MM, Monroe RS, Ohmstede CA. The cDNA sequence and characterization of the Ca2+/calmodulin-dependent protein kinase-Gr from human brain and thymus. Gene. 1994; 142:191–197. [PubMed: 8194751]

Bland MM. Identification of alternate 5' untranslated regions in the gene encoding Ca2+/calmodulin-dependent kinase-G1. Gene. 1993; 137:351–352. [PubMed: 8299971]

Bolognani F, Merhege MA, Twiss J, Perrone-Bizzozero NI. Dendritic localization of the RNA-binding protein HuD in hippocampal neurons: association with polysomes and upregulation during contextual learning. Neurosci Lett. 2004; 371:152–157. [PubMed: 15519747]

Borson ND, Salo WL, Drewes LR. A lock-docking oligo(dT) primer for 5' and 3' RACE PCR. Genome Res. 1992; 2:144–148.

Boyden ES, Katoh A, Pyle JL, Chatila TA, Tsien RW, Raymond JL. Selective engagement of plasticity mechanisms for motor memory storage. Neuron. 2006; 51:823–834. [PubMed: 16982426]

Brumovsky PR, Shi TJ, Matsuda H, Kopp J, Villar MJ, Hökfelt T. NPY Y1 receptors are present in axonal processes of DRG neurons. Exp Neurol. 2002; 174:1–10. [PubMed: 11869028]

Chen CY, Shyu AB. AU-rich elements: characterization and importance in mRNA degradation. Trends Biochem Sci. 1995; 20:465–470. [PubMed: 8578590]

Cook KB, Kazan H, Zuberi K, Morris Q, Hughes TR. RBPDB: a database of RNA-binding specificities. Nucleic Acids Res. 2010; 39:D301–D308. [PubMed: 21036867]

Corcoran EE, Joseph JD, MacDonald JA, Kane CD, Haystead TAJ, Means AR. Proteomic analysis of calcium/calmodulin-dependent protein kinase I and IV in vitro substrates reveals distinct catalytic preferences. J Biol Chem. 2003; 278:10516–10522. [PubMed: 12538590]

Cosker KE, Courchesne SL, Segal RA. Action in the axon: generation and transport of signaling endosomes. Curr Opin Neurobiol. 2008; 18:270–275. [PubMed: 18778772]

Costes SV, Daelemans D, Cho EH, Dobbin Z, Pavlakis G, Lockett S. Automatic and quantitative measurement of protein-protein colocalization in live cells. Biophys J. 2004; 86:3993–4003. [PubMed: 15189895]

Deinhardt K, Salinas S, Verastegui C, Watson R, Worth D, Hanrahan S, Bucci C, Schiavo G. Rab5 and Rab7 Control Endocytic Sorting along the Axonal Retrograde Transport Pathway. Neuron. 2006; 52:293–305. [PubMed: 17046692]

Diamond J, Holmes M, Coughlin M. Endogenous NGF and nerve impulses regulate the collateral sprouting of sensory axons in the skin of the adult rat. J Neurosci Off J Soc Neurosci. 1992; 12:1454–1466.

Dobrowolski R, Vick P, Ploper D, Gumper I, Snitkin H, Sabatini DD, De Robertis EM. Presenilin Deficiency or Lysosomal Inhibition Enhances Wnt Signaling through Relocalization of GSK3 to the Late-Endosomal Compartment. Cell Reports. 2012; 2:1316–1328. [PubMed: 23122960]

Dunham I, Kundaje A, Aldred SF, Collins PJ, Davis CA, Doyle F, Epstein CB, Frietze S, Harrow J, Kaul R, et al. An integrated encyclopedia of DNA elements in the human genome. Nature. 2012; 489:57–74. [PubMed: 22955616]

Fainzilber M, Budnik V, Segal RA, Kreutz MR. From Synapse to Nucleus and Back Again—Communication Over Distance Within Neurons. J Neurosci. 2011; 31:16045–16048. [PubMed: 22072654]

Fang X, Djouhri L, McMullan S, Berry C, Waxman SG, Okuse K, Lawson SN. Intense isolectin-B4 binding in rat dorsal root ganglion neurons distinguishes C-fiber nociceptors with broad action potentials and high Nav1.9 expression. J Neurosci Off J Soc Neurosci. 2006; 26:7281–7292.

Fujiwara Y, Kasashima K, Saito K, Fukuda M, Fukao A, Sasano Y, Inoue K, Fujiwara T, Sakamoto H. Microtubule association of a neuronal RNA-binding protein HuD through its binding to the light chain of MAP1B. Biochimie. 2011; 93:817–822. [PubMed: 21288476]

Fundin BT, Arvidsson J, Aldskogius H, Johansson O, Rice SN, Rice FL. Comprehensive immunofluorescence and lectin binding analysis of intervibrissal fur innervation in the mystacial pad of the rat. J Comp Neurol. 1997; 385:185–206. [PubMed: 9268123]

Galoyan SM, Petruska JC, Mendell LM. Mechanisms of sensitization of the response of single dorsal root ganglion cells from adult rat to noxious heat. Eur J Neurosci. 2003; 18:535–541. [PubMed: 12911749]

Gavazzi I, Kumar RD, McMahon SB, Cohen J. Growth responses of different subpopulations of adult sensory neurons to neurotrophic factors in vitro. Eur J Neurosci. 1999; 11:3405–3414. [PubMed: 10564348]

Ghosh T, Soni K, Scaria V, Halimani M, Bhattacharjee C, Pillai B. MicroRNA-mediated up-regulation of an alternatively polyadenylated variant of the mouse cytoplasmic β-actin gene. Nucleic Acids Res. 2008; 36:6318–6332. [PubMed: 18835850]

Di Giammartino DC, Nishida K, Manley JL. Mechanisms and consequences of alternative polyadenylation. Mol Cell. 2011; 43:853–866. [PubMed: 21925375]

Glinka M, Herrmann T, Funk N, Havlicek S, Rossoll W, Winkler C, Sendtner M. The heterogeneous nuclear ribonucleoprotein-R is necessary for axonal beta-actin mRNA translocation in spinal motor neurons. Hum Mol Genet. 2010; 19:1951–1966. [PubMed: 20167579]

Green MF, Scott JW, Steel R, Oakhill JS, Kemp BE, Means AR. Ca2+/Calmodulin-dependent Protein Kinase Kinase β Is Regulated by Multisite Phosphorylation. J Biol Chem. 2011; 286:28066–28079. [PubMed: 21669867]

Hansen MR, Bok J, Devaiah AK, Zha X-M, Green SH. Ca2+/calmodulin-dependent protein kinases II and IV both promote survival but differ in their effects on axon growth in spiral ganglion neurons. J Neurosci Res. 2003; 72:169–184. [PubMed: 12671991]

Hanz S, Perlson E, Willis D, Zheng J-Q, Massarwa R, Huerta JJ, Koltzenburg M, Kohler M, van-Minnen J, Twiss JL, et al. Axoplasmic importins enable retrograde injury signaling in lesioned nerve. Neuron. 2003; 40:1095–1104. [PubMed: 14687545]

Harrison B, Kraus M, Burch L, Stevens C, Craig A, Gordon-Weeks P, Hupp TR. DAPK-1 binding to a linear peptide motif in MAP1B stimulates autophagy and membrane blebbing. J Biol Chem. 2008; 283:9999–10014. [PubMed: 18195017]

Hickey G, Paten B, Earl D, Zerbino D, Haussler D. HAL: A Hierarchical Format for Storing and Analyzing Multiple Genome Alignments. Bioinforma Oxf Engl. 2013

Hill CE, Harrison BJ, Rau KK, Hougland MT, Bunge MB, Mendell LM, Petruska JC. Skin incision induces expression of axonal regeneration-related genes in adult rat spinal sensory neurons. J Pain Off J Am Pain Soc. 2010; 11:1066–1073.

Ho N, Liauw JA, Blaeser F, Wei F, Hanissian S, Muglia LM, Wozniak DF, Nardi A, Arvin KL, Holtzman DM, et al. Impaired Synaptic Plasticity and cAMP Response Element-Binding Protein Activation in Ca2+/Calmodulin-Dependent Protein Kinase Type IV/Gr-Deficient Mice. J Neurosci. 2000; 20:6459–6472. [PubMed: 10964952]

Hoeller D, Volarevic S, Dikic I. Compartmentalization of growth factor receptor signalling. Curr Opin Cell Biol. 2005; 17:107–111. [PubMed: 15780584]

Holmes TJ, Liu YH. Richardson-Lucy/maximum likelihood image restoration algorithm for fluorescence microscopy: further testing. Appl Opt. 1989; 28:4930–4938. [PubMed: 20555971]

Humphries WH, Szymanski CJ, Payne CK. Endo-Lysosomal Vesicles Positive for Rab7 and LAMP1 Are Terminal Vesicles for the Transport of Dextran. Plos One. 2011; 6:e26626. [PubMed: 22039519]

Ince-Dunn G, Okano HJ, Jensen KB, Park W-Y, Zhong R, Ule J, Mele A, Fak JJ, Yang C, Zhang C, et al. Neuronal Elav-like (Hu) Proteins Regulate RNA Splicing and Abundance to Control Glutamate Levels and Neuronal Excitability. Neuron. 2012; 75:1067–1080. [PubMed: 22998874]

Ivanavicius SP, Blake DR, Chessell IP, Mapp PI. Isolectin B4 binding neurons are not present in the rat knee joint. Neuroscience. 2004; 128:555–560. [PubMed: 15381284]

Jensen KF, Ohmstede CA, Fisher RS, Sahyoun N. Nuclear and axonal localization of Ca2+/calmodulin-dependent protein kinase type Gr in rat cerebellar cortex. Proc Natl Acad Sci U S A. 1991; 88:2850–2853. [PubMed: 2011593]

Ji R-R, Shi T-J, Xu Z-Q, Zhang Q, Sakagami H, Tsubochi H, Kondo H, Hökfelt T. Ca2+/calmodulin-dependent protein kinase type IV in dorsal root ganglion: colocalization with peptides, axonal transport and effect of axotomy. Brain Res. 1996; 721:167–173. [PubMed: 8793097]

Jiao X, Chen H, Chen J, Herrup K, Firestein BL, Kiledjian M. Modulation of Neuritogenesis by a Protein Implicated in X-Linked Mental Retardation. J Neurosci. 2009; 29:12419–12427. [PubMed: 19812318]

Kamata A, Sakagami H, Tokumitsu H, Sanda M, Owada Y, Fukunaga K, Kondo H. Distinct developmental expression of two isoforms of Ca2+/calmodulin-dependent protein kinase kinases and their involvement in hippocampal dendritic formation. Neurosci Lett. 2007; 423:143–148. [PubMed: 17669591]

Kang H, Sun LD, Atkins CM, Soderling TR, Wilson MA, Tonegawa S. An important role of neural activity-dependent CaMKIV signaling in the consolidation of long-term memory. Cell. 2001; 106:771–783. [PubMed: 11572782]

Kankaanpää P, Paavolainen L, Tiitta S, Karjalainen M, Päivärinne J, Nieminen J, Marjomäki V, Heino J, White DJ. BioImageXD: an open, general-purpose and high-throughput image-processing platform. Nat Methods. 2012; 9:683–689. [PubMed: 22743773]

Kent WJ, Sugnet CW, Furey TS, Roskin KM, Pringle TH, Zahler AM, Haussler D. The human genome browser at UCSC. Genome Res. 2002; 12:996–1006. [PubMed: 12045153]

Kitao Y, Robertson B, Kudo M, Grant G. Proliferation patterns of dorsal root ganglion neurons of cutaneous, muscle and visceral nerves in the rat. J Neurocytol. 2002; 31:765–776. [PubMed: 14501213]

Kotera I, Sekimoto T, Miyamoto Y, Saiwaki T, Nagoshi E, Sakagami H, Kondo H, Yoneda Y. Importin α transports CaMKIV to the nucleus without utilizing importin β. Embo J. 2005; 24:942–951. [PubMed: 15719015]

Kuniyoshi K, Ohtori S, Ochiai N, Murata R, Matsudo T, Yamada T, Ochiai SS, Moriya H, Takahashi K. Characteristics of sensory DRG neurons innervating the wrist joint in rats. Eur J Pain Lond Engl. 2007; 11:323–328.

Lasiecka ZM, Winckler B. Mechanisms of polarized membrane trafficking in neurons -- focusing in on endosomes. Mol Cell Neurosci. 2011; 48:278–287. [PubMed: 21762782]

Lawson SN. Phenotype and function of somatic primary afferent nociceptive neurones with C-, Adelta- or Aalpha/beta-fibres. Exp Physiol. 2002; 87:239–244. [PubMed: 11856969]

Leitner ML, Molliver DC, Osborne PA, Vejsada R, Golden JP, Lampe PA, Kato AC, Milbrandt J, Johnson EM Jr. Analysis of the retrograde transport of glial cell line-derived neurotrophic factor (GDNF), neurturin, and persephin suggests that in vivo signaling for the GDNF family is GFRalpha coreceptor-specific. J Neurosci Off J Soc Neurosci. 1999; 19:9322–9331.

Lemrow SM, Anderson KA, Joseph JD, Ribar TJ, Noeldner PK, Means AR. Catalytic Activity Is Required for Calcium/Calmodulin-dependent Protein Kinase IV to Enter the Nucleus. J Biol Chem. 2004; 279:11664–11671. [PubMed: 14701808]

Lin F, Ribar TJ, Means AR. The Ca2+/Calmodulin-Dependent Protein Kinase Kinase, CaMKK2, Inhibits Preadipocyte Differentiation. Endocrinology. 2011; 152:3668–3679. [PubMed: 21862616]

Lopez F, Granjeaud S, Ara T, Ghattas B, Gautheret D. The disparate nature of “intergenic” polyadenylation sites. Rna New York N. 2006; 12:1794–1801.

Malin SA, Molliver DC, Koerber HR, Cornuet P, Frye R, Albers KM, Davis BM. Glial cell line-derived neurotrophic factor family members sensitize nociceptors in vitro and produce thermal hyperalgesia in vivo. J Neurosci Off J Soc Neurosci. 2006; 26:8588–8599.

Marie H, Morishita W, Yu X, Calakos N, Malenka RC. Generation of silent synapses by acute in vivo expression of CaMKIV and CREB. Neuron. 2005; 45:741–752. [PubMed: 15748849]

Marshall OJ. PerlPrimer: cross-platform, graphical primer design for standard, bisulphite and real-time PCR. Bioinforma Oxf Engl. 2004; 20:2471–2472.

Mattick JS. The central role of RNA in human development and cognition. Febs Lett. 2011; 585:1600–1616. [PubMed: 21557942]

Mayford M, Baranes D, Podsypanina K, Kandel ER. The 3′-untranslated region of CaMKIIα is a cis-acting signal for the localization and translation of mRNA in dendrites. Proc Natl Acad Sci. 1996; 93:13250–13255. [PubMed: 8917577]

Meisner N-C, Filipowicz W. Properties of the Regulatory RNA-Binding Protein HuR and its Role in Controlling miRNA Repression. Adv Exp Med Biol. 2011; 700:106–123. [PubMed: 21755477]

Melander Gradin H, Marklund U, Larsson N, Chatila TA, Gullberg M. Regulation of microtubule dynamics by Ca2+/calmodulin-dependent kinase IV/Gr-dependent phosphorylation of oncoprotein 18. Mol Cell Biol. 1997; 17:3459–3467. [PubMed: 9154845]

Molliver DC, Wright DE, Leitner ML, Parsadanian AS, Doster K, Wen D, Yan Q, Snider WD. IB4-binding DRG neurons switch from NGF to GDNF dependence in early postnatal life. Neuron. 1997; 19:849–861. [PubMed: 9354331]

Moucadel V, Lopez F, Ara T, Benech P, Gautheret D. Beyond the 3' end: experimental validation of extended transcript isoforms. Nucleic Acids Res. 2007; 35:1947–1957. [PubMed: 17339231]

Muddashetty RS, Kelić S, Gross C, Xu M, Bassell GJ. Dysregulated Metabotropic Glutamate Receptor-Dependent Translation of AMPA Receptor and Postsynaptic Density-95 mRNAs at Synapses in a Mouse Model of Fragile X Syndrome. J Neurosci. 2007; 27:5338–5348. [PubMed: 17507556]

Nagendran T, Hardy LR. Calcium/calmodulin-dependent protein kinase IV mediates distinct features of basal and activity-dependent dendrite complexity. Neuroscience. 2011; 199:548–562. [PubMed: 21989476]

Nakajima T, Ohtori S, Inoue G, Koshi T, Yamamoto S, Nakamura J, Takahashi K, Harada Y. The characteristics of dorsal-root ganglia and sensory innervation of the hip in rats. J Bone Joint Surg Br. 2008; 90:254–257. [PubMed: 18256100]

Nakamura Y, Okuno S, Sato F, Fujisawa H. An immunohistochemical study of Ca2+/calmodulin-dependent protein kinase IV in the rat central nervous system: light and electron microscopic observations. Neuroscience. 1995; 68:181–194. [PubMed: 7477923]

Neal AP, Molina-Campos E, Marrero-Rosado B, Bradford AB, Fox SM, Kovalova N, Hannon HE. CaMKK-CaMKI signaling pathways differentially control axon and dendrite elongation in cortical neurons. J Neurosci Off J Soc Neurosci. 2010; 30:2807–2809.

Neilson JR, Sandberg R. Heterogeneity in mammalian RNA 3' end formation. Exp Cell Res. 2010; 316:1357–1364. [PubMed: 20211174]

Newnham CM, Hall-Pogar T, Liang S, Wu J, Tian B, Hu J, Lutz CS. Alternative polyadenylation of MeCP2: influence of cis-acting elements and trans-acting factors. Rna Biol. 2010; 7:361–372. [PubMed: 20400852]

Oh U, Hwang SW, Kim D. Capsaicin activates a nonselective cation channel in cultured neonatal rat dorsal root ganglion neurons. J Neurosci Off J Soc Neurosci. 1996; 16:1659–1667.

Okano HJ, Darnell RB. A hierarchy of Hu RNA binding proteins in developing and adult neurons. J Neurosci Off J Soc Neurosci. 1997; 17:3024–3037.

Di Paolo G, Pellier V, Catsicas M, Antonsson B, Catsicas S, Grenningloh G. The phosphoprotein stathmin is essential for nerve growth factor-stimulated differentiation. J Cell Biol. 1996; 133:1383–1390. [PubMed: 8682872]

Pascale A, Amadio M, Quattrone A. Defining a neuron: neuronal ELAV proteins. Cell Mol Life Sci Cmls. 2008; 65:128–140.

Pascale A, Gusev PA, Amadio M, Dottorini T, Govoni S, Alkon DL, Quattrone A. Increase of the RNA-binding protein HuD and posttranscriptional up-regulation of the GAP-43 gene during spatial memory. Proc Natl Acad Sci U S A. 2004; 101:1217–1222. [PubMed: 14745023]

Peng SS, Chen CY, Xu N, Shyu AB. RNA stabilization by the AU-rich element binding protein, HuR, an ELAV protein. Embo J. 1998; 17:3461–3470. [PubMed: 9628881]

Perlson E, Hanz S, Ben-Yaakov K, Segal-Ruder Y, Seger R, Fainzilber M. Vimentin-dependent spatial translocation of an activated MAP kinase in injured nerve. Neuron. 2005; 45:715–726. [PubMed: 15748847]

Petruska JC, Cooper BY, Gu JG, Rau KK, Johnson RD. Distribution of P2X1, P2X2, and P2X3 receptor subunits in rat primary afferents: relation to population markers and specific cell types. J Chem Neuroanat. 2000a; 20:141–162. [PubMed: 11118807]

Petruska JC, Napaporn J, Johnson RD, Cooper BY. Chemical responsiveness and histochemical phenotype of electrophysiologically classified cells of the adult rat dorsal root ganglion. Neuroscience. 2002; 115:15–30. [PubMed: 12401318]

Petruska JC, Napaporn J, Johnson RD, Gu JG, Cooper BY. Subclassified acutely dissociated cells of rat DRG: histochemistry and patterns of capsaicin-, proton-, and ATP-activated currents. J Neurophysiol. 2000b; 84:2365–2379. [PubMed: 11067979]

Petruska JC, Streit WJ, Johnson RD. Localization of unmyelinated axons in rat skin and mucocutaneous tissue utilizing the isolectin GS-I-B4. Somatosens Mot Res. 1997; 14:17–26. [PubMed: 9241725]

Pizon V, Desjardins M, Bucci C, Parton RG, Zerial M. Association of Rap1a and Rap1b proteins with late endocytic/phagocytic compartments and Rap2a with the Golgi complex. J Cell Sci. 1994; 107(Pt 6):1661–1670. [PubMed: 7962206]

Poëa-Guyon S, Amar M, Fossier P, Morel N. Alternative splicing controls neuronal expression of v-ATPase subunit a1 and sorting to nerve terminals. J Biol Chem. 2006; 281:17164–17172. [PubMed: 16621796]

Raju CS, Göritz C, Nord Y, Hermanson O, López-Iglesias C, Visa N, Castelo-Branco G, Percipalle P. In cultured oligodendrocytes the A/B-type hnRNP CBF-A accompanies MBP mRNA bound to mRNA trafficking sequences. Mol Biol Cell. 2008; 19:3008–3019. [PubMed: 18480411]

Ramarli D, Fox DA, Milanese C, Reinherz EL. Selective inhibition of interleukin 2 gene function following thymocyte antigen/major histocompatibility complex receptor crosslinking: possible thymic selection mechanism. Proc Natl Acad Sci U S A. 1986; 83:7008–7012. [PubMed: 3489236]

Rau KK, Jiang N, Johnson RD, Cooper BY. Heat sensitization in skin and muscle nociceptors expressing distinct combinations of TRPV1 and TRPV2 protein. J Neurophysiol. 2007; 97:2651–2662. [PubMed: 17287441]

Redmond L, Kashani AH, Ghosh A. Calcium regulation of dendritic growth via CaM kinase IV and CREB-mediated transcription. Neuron. 2002; 34:999–1010. [PubMed: 12086646]

Rice FL. Structure, vascularization, and innervation of the mystacial pad of the rat as revealed by the lectin Griffonia simplicifolia. J Comp Neurol. 1993; 337:386–399. [PubMed: 8282849]

Richardson DS, Lai AZ, Mulligan LM. RET ligand-induced internalization and its consequences for downstream signaling. Oncogene. 2006; 25:3206–3211. [PubMed: 16418724]

Rosenbaum T, Gordon-Shaag A, Munari M, Gordon SE. Ca2+/calmodulin modulates TRPV1 activation by capsaicin. J Gen Physiol. 2004; 123:53–62. [PubMed: 14699077]

Rossoll W, Jablonka S, Andreassi C, Kröning A-K, Karle K, Monani UR, Sendtner M. Smn, the spinal muscular atrophy-determining gene product, modulates axon growth and localization of beta-actin mRNA in growth cones of motoneurons. J Cell Biol. 2003; 163:801–812. [PubMed: 14623865]

Sahyoun N, McDonald OB, Farrell F, Lapetina EG. Phosphorylation of a Ras-related GTP-binding protein, Rap-1b, by a neuronal Ca2+/calmodulin-dependent protein kinase, CaM kinase Gr. Proc Natl Acad Sci U S A. 1991; 88:2643–2647. [PubMed: 1901412]

Sakagami H, Umemiya M, Kobayashi T, Saito S, Kondo H. Immunological evidence that the beta isoform of Ca2+/calmodulin-dependent protein kinase IV is a cerebellar granule cell-specific product of the CaM kinase IV gene. Eur J Neurosci. 1999; 11:2531–2536. [PubMed: 10383642]

Saneyoshi T, Wayman G, Fortin D, Davare M, Hoshi N, Nozaki N, Natsume T, Soderling TR. Activity-dependent synaptogenesis: regulation by a CaM-kinase kinase/CaM-kinase I/betaPIX signaling complex. Neuron. 2008; 57:94–107. [PubMed: 18184567]

Saxena S, Bucci C, Weis J, Kruttgen A. The Small GTPase Rab7 Controls the Endosomal Trafficking and Neuritogenic Signaling of the Nerve Growth Factor Receptor TrkA. J Neurosci. 2005; 25:10930–10940. [PubMed: 16306406]

Schindelin J, Arganda-Carreras I, Frise E, Kaynig V, Longair M, Pietzsch T, Preibisch S, Rueden C, Saalfeld S, Schmid B, et al. Fiji: an open-source platform for biological-image analysis. Nat Methods. 2012; 9:676–682. [PubMed: 22743772]

Shaw G, Kamen R. A conserved AU sequence from the 3' untranslated region of GM-CSF mRNA mediates selective mRNA degradation. Cell. 1986; 46:659–667. [PubMed: 3488815]

Shu X, Mendell LM. Acute sensitization by NGF of the response of small-diameter sensory neurons to capsaicin. J Neurophysiol. 2001; 86:2931–2938. [PubMed: 11731549]

Sievers F, Wilm A, Dineen D, Gibson TJ, Karplus K, Li W, Lopez R, McWilliam H, Remmert M, Söding J, et al. Fast, scalable generation of high-quality protein multiple sequence alignments using Clustal Omega. Mol Syst Biol. 2011; 7:539. [PubMed: 21988835]

De Souza N. The ENCODE project. Nat Methods. 2012; 9:1046. [PubMed: 23281567]

Spencer TK, Mellado W, Filbin MT. BDNF activates CaMKIV and PKA in parallel to block MAG-mediated inhibition of neurite outgrowth. Mol Cell Neurosci. 2008; 38:110–116. [PubMed: 18381242]

Stewart HJ. Expression of c-Jun, Jun B, Jun D and cAMP response element binding protein by Schwann cells and their precursors in vivo and in vitro. Eur J Neurosci. 1995; 7:1366–1375. [PubMed: 7582111]

Streit WJ, Schulte BA, Spicer SS, Balentine JD. Histochemical localization of galactose-containing glycoconjugate at peripheral nodes of Ranvier in the rat. J Histochem Cytochem Off J Histochem Soc. 1985; 33:33–39.

Sun Z, Means RL, LeMagueresse B, Means AR. Organization and Analysis of the Complete Rat Calmodulin-dependent Protein Kinase IV Gene. J Biol Chem. 1995; 270:29507–29514. [PubMed: 7493991]

Tai Y, Feng S, Ge R, Du W, Zhang X, He Z, Wang Y. TRPC6 channels promote dendritic growth via the CaMKIV-CREB pathway. J Cell Sci. 2008; 121:2301–2307. [PubMed: 18559891]

Takemura M, Mishima T, Wang Y, Kasahara J, Fukunaga K, Ohashi K, Mizuno K. Ca2+/calmodulin-dependent protein kinase IV-mediated LIM kinase activation is critical for calcium signal-induced neurite outgrowth. J Biol Chem. 2009; 284:28554–28562. [PubMed: 19696021]

Tian B, Hu J, Zhang H, Lutz CS. A large-scale analysis of mRNA polyadenylation of human and mouse genes. Nucleic Acids Res. 2005; 33:201–212. [PubMed: 15647503]

Verge VM, Richardson PM, Benoit R, Riopelle RJ. Histochemical characterization of sensory neurons with high-affinity receptors for nerve growth factor. J Neurocytol. 1989; 18:583–591. [PubMed: 2559166]

Wang H, Rivero-Melián C, Robertson B, Grant G. Transganglionic transport and binding of the isolectin B4 from Griffonia simplicifolia I in rat primary sensory neurons. Neuroscience. 1994; 62:539–551. [PubMed: 7530347]

Wang HF, Robertson B, Grant G. Anterograde transport of horseradish-peroxidase conjugated isolectin B4 from Griffonia simplicifolia I in spinal primary sensory neurons of the rat. Brain Res. 1998a; 811:34–39. [PubMed: 9804881]

Wang HF, Shortland P, Park MJ, Grant G. Retrograde and transganglionic transport of horseradish peroxidase-conjugated cholera toxin B subunit, wheatgerm agglutinin and isolectin B4 from Griffonia simplicifolia I in primary afferent neurons innervating the rat urinary bladder. Neuroscience. 1998b; 87:275–288. [PubMed: 9722157]

Wayman GA, Impey S, Marks D, Saneyoshi T, Grant WF, Derkach V, Soderling TR. Activity-dependent dendritic arborization mediated by CaM-kinase I activation and enhanced CREB-dependent transcription of Wnt-2. Neuron. 2006; 50:897–909. [PubMed: 16772171]

Wayman GA, Kaech S, Grant WF, Davare M, Impey S, Tokumitsu H, Nozaki N, Banker G, Soderling TR. Regulation of axonal extension and growth cone motility by calmodulin-dependent protein kinase I. J Neurosci Off J Soc Neurosci. 2004; 24:3786–3794.

Wayman GA, Lee Y-S, Tokumitsu H, Silva A, Soderling TR. Calmodulin-Kinases: Modulators of Neuronal Development and Plasticity. Neuron. 2008; 59:914–931. [PubMed: 18817731]

Wayman GA, Tokumitsu H, Davare MA, Soderling TR. Analysis of CaM-kinase Signaling in Cells. Cell Calcium. 2011; 50:1–8. [PubMed: 21529938]

Willis DE, van Niekerk EA, Sasaki Y, Mesngon M, Merianda TT, Williams GG, Kendall M, Smith DS, Bassell GJ, Twiss JL. Extracellular stimuli specifically regulate localized levels of individual neuronal mRNAs. J Cell Biol. 2007; 178:965–980. [PubMed: 17785519]

Willis DE, Xu M, Donnelly CJ, Tep C, Kendall M, Erenstheyn M, English AW, Schanen NC, Kirn-Safran CB, Yoon SO, et al. Axonal Localization of transgene mRNA in mature PNS and CNS neurons. J Neurosci Off J Soc Neurosci. 2011; 31:14481–14487.

Wu JY, Ribar TJ, Cummings DE, Burton KA, McKnight GS, Means AR. Spermiogenesis and exchange of basic nuclear proteins are impaired in male germ cells lacking Camk4. Nat Genet. 2000; 25:448–452. [PubMed: 10932193]

Ben-Yaakov K, Dagan SY, Segal-Ruder Y, Shalem O, Vuppalanchi D, Willis DE, Yudin D, Rishal I, Rother F, Bader M, et al. Axonal transcription factors signal retrogradely in lesioned peripheral nerve. Embo J. 2012; 31:1350–1363. [PubMed: 22246183]

Yu J, Hai Y, Liu G, Fang T, Kung SKP, Xie J. The heterogeneous nuclear ribonucleoprotein L is an essential component in the Ca2+/calmodulin-dependent protein kinase IV-regulated alternative splicing through cytidine-adenosine repeats. J Biol Chem. 2009; 284:1505–1513. [PubMed: 19017650]

Zylka MJ, Rice FL, Anderson DJ. Topographically distinct epidermal nociceptive circuits revealed by axonal tracers targeted to Mrgprd. Neuron. 2005; 45:17–25. [PubMed: 15629699]

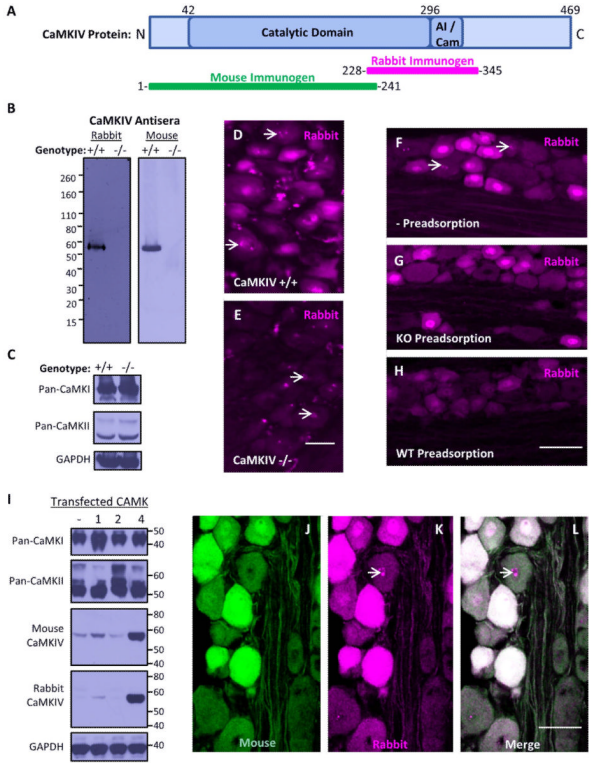

Figure 1. Validation of 2 commercially available CaMKIV antibodies

A: The commercially obtained antibodies used in this study were developed using immunogens derived from separate regions of the catalytic domain of CaMKIV. N = amino terminus, C = carboxy terminus, numbers are amino acid positions. AI/Cam = Autoinhibitory/Calmodulin-binding domain.

B: Western blot of DRG homogenates from *CaMK4* knock-out (−/−) and wild-type (+/+) mice. Entire representative blots using either rabbit or mouse antisera are shown.

C: Protein levels of CaMK family members in the same lysates as in **B**. Note that these proteins were not affected by *CaMK4* gene ablation. GAPDH antibody was used as a loading control.

D–E: Immunofluorescence micrographs of wild-type vs *CaMK4* knock-out mouse DRG sections using rabbit antisera. Arrow heads show staining not affected by gene ablation. Scale bar = 30μm

F: Rat DRG section stained with rabbit antisera. Arrow heads are non-specific signals within neuronal nuclei as determined in **E**.

G: Rat DRG section stained with rabbit antisera preadsorbed with *CaMK4*-KO mouse brain lysate. Note that background signals are removed.

H: Rat DRG section stained with rabbit antisera preadsorbed with *CaMK4*-WT mouse brain lysate. Note that all signals are uniformly reduced. Scale bar = 40μm

I: Protein lysates from PC12 cells transfected with *CaMK1*, *CaMK2*, or *CaMK4* and assayed by Western blotting. Note that cross-reaction with these related proteins was not observed with either rabbit or mouse antisera.

J–L: Multichannel immunofluorescence images of 14μM rat DRG sections co-stained with both rabbit and mouse antibodies. Note that both antisera stained essentially identical structures. Arrow heads are background signals from the rabbit antisera detailed in **E**. Scale bar = 30μm.

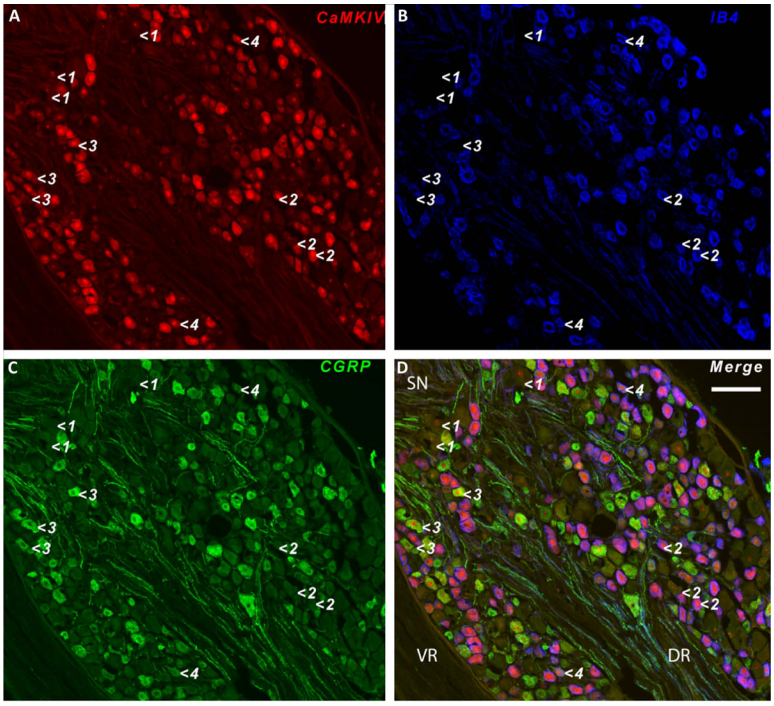

Figure 2. CaMKIV immunofluorescence in neuronal subpopulations of adult rat DRG

14μm rat DRG section stained with Rabbit CaMKIV (**A** Red). CGRP was used to co-stain neuropeptide-expressing neurons (**B** Green) and isolectin IB4 (**C** Blue) used to co-stain cutaneous nociceptors. **D** = merged image. Open arrows are representative cells from the following populations: IB4−/CGRP− (1), IB4+/CGRP− (2), IB4−/CGRP+ (3) and IB4+/CGRP+ (4). DR = Dorsal Root, VR = Ventral Root, SN = Spinal Nerve. Scale bar = 100μm.

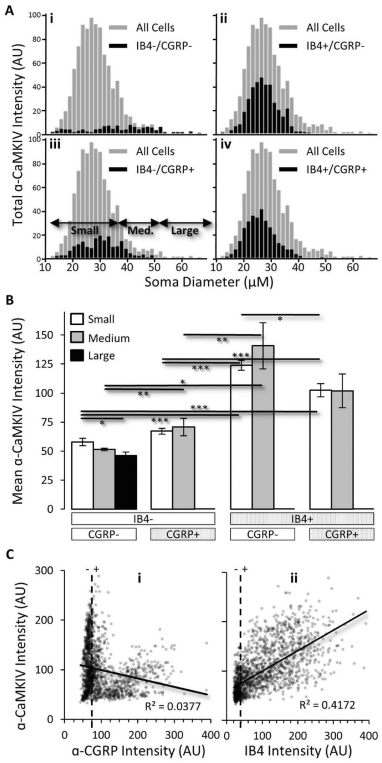

Figure 3. Quantitative analysis of CaMKIV staining intensity in sub-populations of DRG neurons

14μM DRG sections were stained from 4 separate animals, 2 sections per animal. All cells with a visible nucleus were included in the analysis (total of 1800 cells).

A: Total CaMKIV intensity (y axis) vs neuron diameter (x axis, 2μM bin size). The entire neuron population (grey background bars) and individual populations (i IB4−/CGRP−, ii IB4+/CGRP−, iii IB4−/CGRP+ and iv IB4+/CGRP+) were analysed. Mean CaMKIV signal in each population: IB4−/CGRP− 5.8%, IB4−/CGRP+ 13.3%, IB4+/CGRP− 47.9% and IB4+/CGRP+ 33.0%.

B: Mean average CaMKIV intensity in small (<35μM), medium (35–50μM) and large (>50μM) diameter neurons. n=4 animals (450 cells/animal), groups compared using oneway ANOVA with Tukey HSD post hoc ttests. Horizontal lines: The left and right ends of each line center on the 2 vertical bars of compared conditions. No line = not significant, * = $p<0.05$, ** = $p<0.01$, *** = $p<0.001$.

C: Scatter plots of CaMKIV intensity values from all analysed cells. Note that when all cells were considered CGRP (i) intensity did not correlate with CaMKIV whereas IB4 intensity positively correlated with CaMKIV intensity (ii).

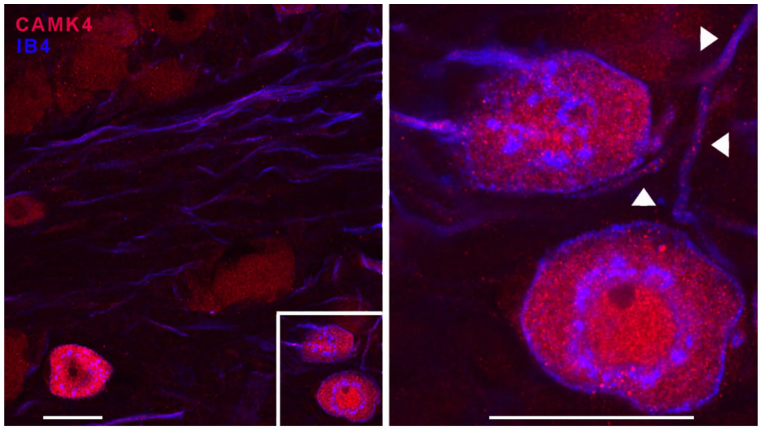

Figure 4. Punctate CaMKIV immunoreactivity within the nuclei, cytoplasm and axons of IB4^{+} nociceptors

Confocal z-slice of rat DRG section stained with mouse CaMKIV antisera (red) and IB4 (cutaneous nociceptors - blue). Inset shows detail of IB4+ soma/axons where arrows are IB4+ axons containing CaMKIV puncta. Scale bar = 25μm.

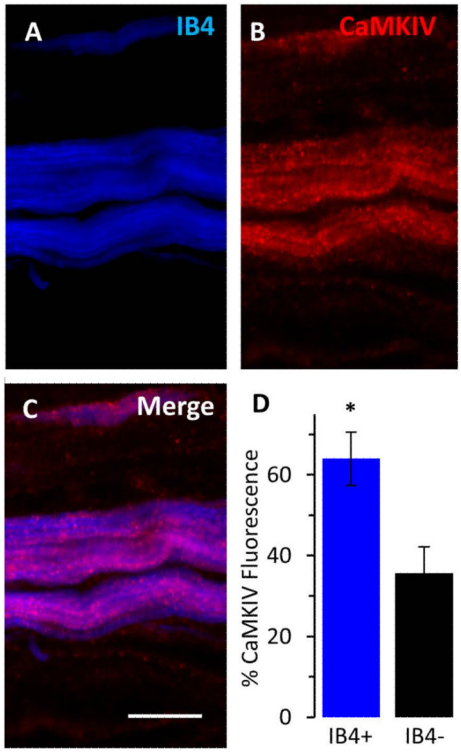

Figure 5. Quantification of CaMKIV immunoreactivity within cutaneous nociceptors of spinal nerve

A–C: Confocal z-slice of rat spinal nerve co-stained with IB4 (cutaneous nociceptors –Blue) and CaMKIV antisera (Red).

D: 62% of CaMKIV fluorescence signal co-located with IB4. Scale bar = 5 μm. * = paired ttest $p<0.05$.

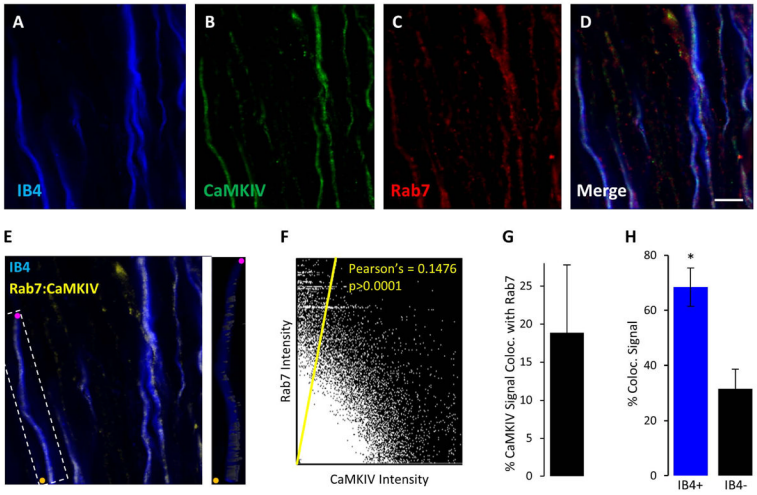

Figure 6. Quantitative colocalisation analyses of CaMKIV immunoreactivity with the endosome marker Rab7 in spinal nerve

A–D: Representative deconvolved confocal z-stack projections through spinal nerve co-stained with IB4 (cutaneous nociceptors – Blue), CaMKIV (green) and Rab7 (red). Scale bar = 5 μm

E: Deconvolved z-stack showing Rab7:CaMKIV colocalised voxels (yellow) using a 3D surface rendering. Inset shows detail from a representative axon (colour dots are registration points).

F: Pearson's correlation of Rab7 vs CaMKIV above threshold voxel intensities determined by Costes' test.

G: % total CaMKIV signal that is colocalised with Rab7 in spinal nerve.

H: % of total colocalised CaMKIV signals in IB4+ axons in spinal nerve.

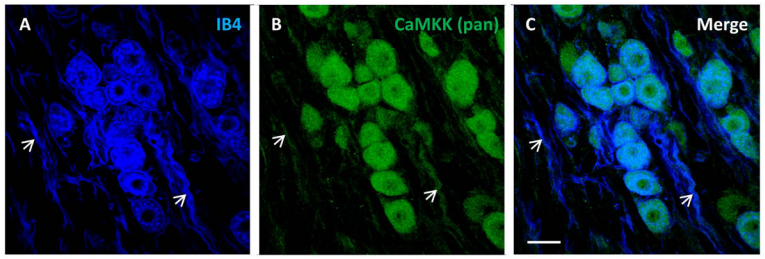

Figure 7. CaMKK expression in DRG

A–C Confocal z-stack through rat DRG co-stained with IB4 (blue) and pan-CAMKK antibody (recognizing both CaMKK 1 and 2). Arrow heads are $CaMKK^{+}/IB4^{+}$ axons. Scale bar = 25μm

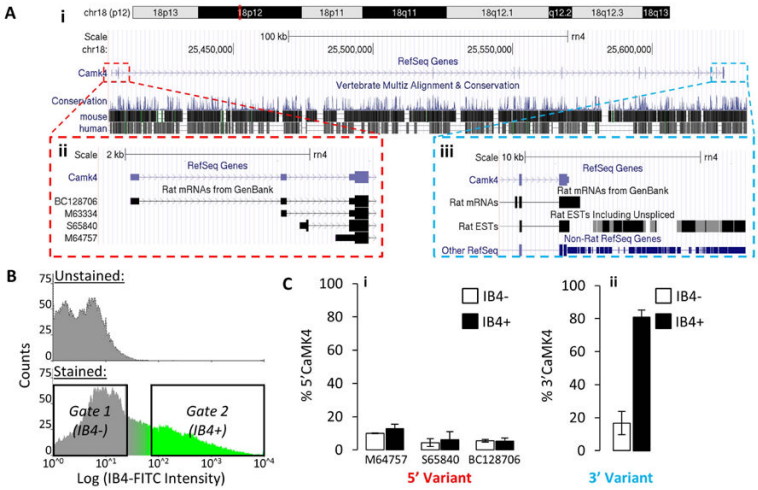

Figure 8. Expression analysis of *CaMK4* mRNA variants in IB4$^+$ DRG neurons: Expression of a putative 3'-untranslated extension in cutaneous nociceptors

A: (i) UCSC Genome Browser output showing the genomic region of rat *CaMK4* including introns (chevrons) and exons (vertical bars). The extent of vertebrate genome sequence conservation is represented on the bottom track with mouse and human detailed. (ii) The genbank RefSeq sequence is curated from mRNA clone sequences submitted (BC128706, M63334, S65840 and M4757). These include the sequence for the *CaMK4*-β isoform (S65840) which adds an extension to the protein N-terminus. (iii) Detail of the 3' end of CaMKIV plus 10kb downstream. A dense representation of all rat expressed sequence tag data from this region is shown (Rat EST) along with a dense representation of homologous non-rat *CaMK4* genes (Other RefSeq).

B: Adult rat DRGs were extracted and dissociated for IB4 staining in cell suspension. Cells were then sorted by FACS into IB4$^+$ (Gate 2) and IB4$^-$ (Gate 1) populations for gene expression analysis.

C: (i) The mRNA expression level of each 5' variant was compared to the expression level of *CaMK4*-α (5'*CaMK4* - M63334) in IB4$^+$ and IB4$^-$ FACS sorted cells using QPCR. (ii) The expression level of cDNA mapping 4kb 3' to the *CaMK4* stop codon (3'*CaMK4*) was compared to the expression level of the last coding exon. In IB4$^+$ cells, this region was expressed to 80% of the level of the last exon.

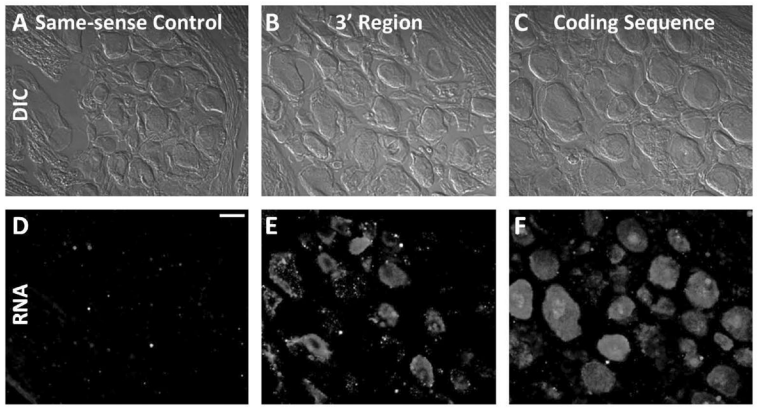

Figure 9. Validation of *CaMK4* 3' isoform expression using *in situ* fluorescence

A–F: Fluorescence *in situ* histofluorescence using riboprobes designed to target the novel 3'-extended transcript exclusively (**B,E**) or all transcripts containing the protein coding sequence (**C,F**). Same-sense riboprobe was used as a negative control (**A,D**). Scale bar = 20μm

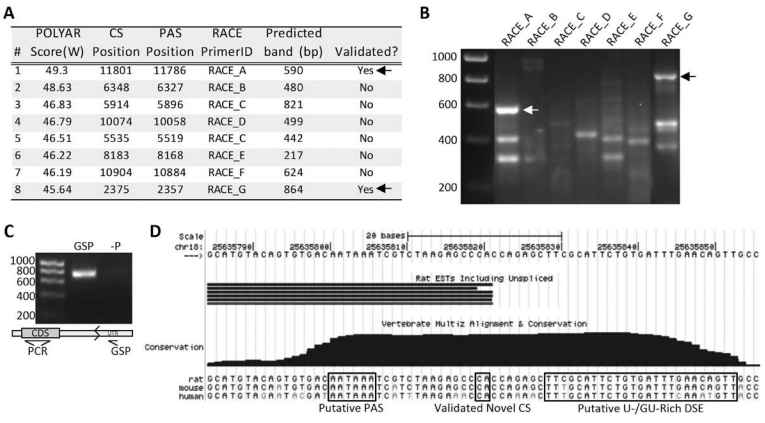

#	POLYAR Score(W)	CS Position	PAS Position	RACE PrimerID	Predicted band (bp)	Validated?
1	49.3	11801	11786	RACE_A	590	Yes ◄
2	48.63	6348	6327	RACE_B	480	No
3	46.83	5914	5896	RACE_C	821	No
4	46.79	10074	10058	RACE_D	499	No
5	46.51	5535	5519	RACE_C	442	No
6	46.22	8183	8168	RACE_E	217	No
7	46.19	10904	10884	RACE_F	624	No
8	45.64	2375	2357	RACE_G	864	Yes ◄

Figure 10. Characterization of a novel 3'UTR extended *CaMK4* mRNA transcript expressed in rat cutaneous nociceptors

A: Summary table of alternate polyadenylation signal characterisation experiments: The POLYAR algorithm was used to predict the position of polyadenylation signals on the final exon of *CaMK4* +12kb downstream. Integral (W) scores, cleavage site (CS) and polyadenylation specificity signal (PAS) positions are relative to the start codon. Rapid amplification of cDNA ends (RACE) was performed using 7 distinct primers designed 200–900bp upstream of the predicated cleavage site.

B: PCR products were separated by electrophoresis and any observable bands excised for sequencing. Bands with sequences that mapped to *CaMK4* were validated polyadenylation sites (arrows).

C: To determine if the extended UTR region was contiguous with the coding sequence (CDS), we designed a gene specific primer (GSP) to prime the cDNA synthesis reaction. PCR probing the kinase domain of *CaMK4* demonstrated that the extended UTR was part of the same transcript as the CDS. cDNA synthesised without primer (-P) was employed as a negative control.

D: UCSC genome browser track centered on the validated polyadenylation site discovered using primer RACE_7. A cluster of expressed sequence tags (ESTs - black lines) terminate at this highly conserved CS which is ≈ 10kb downstream of the CaMKIV stop codon. The CS is flanked by conserved putative PAS and U-/GU-rich down-stream element (DSE) sequence motifs.

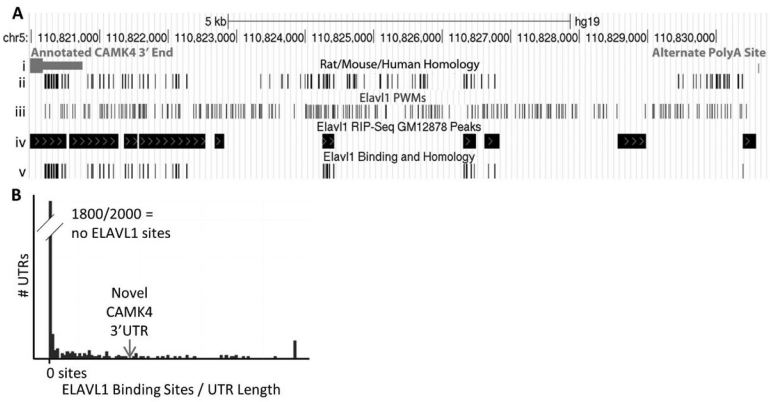

Figure 11. Bioinformatic analysis of ELAVL1 (HuR) RNA-binding protein sites mapping to the 3'UTR of *CaMK4*

A: Conserved ELAVL1 RNA-protein binding sites within the homologous region of the novel *CaMK4* 3'UTR in the human, viewed using the UCSC track genome browser. (i) Position of the 3' end of the *CaMK4* refseq and novel alternate polyA site. (ii) Regions of sequence homology between the human, rat and mouse determined by Clustal Omega three-way alignment. (iii) Elavl1 PWM matches. (iv) Elavl1 RIP-Seq peaks from publically available data (data set GM12878). (v) Intersection of the Rat/Mouse/Human homologous regions and the Elavl1 RIP-Seq data.

B: Comparison of Elavl1 binding peaks in the novel *CaMK4* 3'UTR and 2000 randomly selected rat 3'UTRs of Ensmbl transcripts. The *CaMK4* 3'UTR is indicated by the arrow. Only 2% of rat UTRs have more Elavl1 binding sites.

Table 1

Antibodies used for Western blotting and immunofluorescence studies (Green et al., 2011; Lin et al., 2011; Dobrowolski et al., 2012; Humphries et al., 2011; Jiao et al., 2009; Brumovsky et al., 2002).

Antigen	Immunogen	Manufacturer	Dilution used
CaMKIV	Recombinant human CaMKIV (NP_001735.1) 228–345	Rabbit, polyclonal, Sigma, Cat#HPA017206	IF 1:400 / WB 1:500
CaMKIV	Recombinant human CaMKIV (NP_001735.1) 1–241	Mouse, monoclonal, BD Transduction Laboratories, Cat#610275, Lot#46881	IF 1:1000 / WB 1:2000
Pan-CaMKK	Recombinant rat CaMKK (NP_113850.1) 341–504	Mouse, monoclonal, BD Transduction Laboratories Cat#610545, Lot#23383	IF 1:50
Rab7	Synthetic peptide: CTEVELYNEFPEPIKLDKNDR	Rabbit, monoclonal, Cell Signalling, Cat#9367	IF 1:200
CGRP	Synthetic peptide: ACDTATCVTHRLAGLLSRSGGVVKNNFVPTNVGSKAF	Guinea pig, polyclonal, Fitzgerald, Cat#20R-CP007, Lot#P10031829	IF 1:1500
Pan-CaMKI	Synthetic peptide: MLGAVEGPRWKQAEC	Rabbit, monoclonal, Abcam, Cat#ab68234, Lot#GR9726-3	WB 1:1000
Pan-CaMKII	Synthetic Peptide: CGTPGYLSPEVLRKEAYGK	Rabbit, monoclonal, Cell Signalling Cat#4436, Lot#1	WB 1:1000
GAPDH	GAPDH protein purified from rabbit muscle	Mouse, monoclonal, Cat#Mab374, Lot#JC1604282	WB 1:2000

Table 2

QPCR probes

***CaMK4* Variant**	**Forward Sequence**	**Reverse Sequence**
Total *CaMK4*	CTGACTACATTCCAAGCCC	GATGTTGGTGTGACTGCT
BC1287061	ACATCTCAAGACTTCCAGTG	ATTTGTCATCTCTGCTGGTG
M64757.1	TCACGGTCTCAGCATCTC	AACACAGGAGCGAGAGGA
S65840.1	CTCCAGGAAACATGAGTTGC	CGTGACTTTGAGCATCTTCG
Extended UTR	GGCTCTGAAAACCTGACTGC	ACCGCCATCATAACATACCC

Table 3

RACE primers

Primer ID	Sequence
RT Primer	AATACGACTCACTATAGGGTTTTTTTTTTTTTTTVN
Adaptor Primer	AATACGACTCACTATAGGGTTTT
RACE_A	GATTCCTTAATACAAAGACAGAAT
RACE_B	ATGGGTATGTTATGATGGCGG
RACE_C	CCCAGACTCAAACTCACAC
RACE_D	TATCTGCCTTAAGGGAACCA
RACE_E	TGGCATAGATGTAGTCTGTC
RACE_F	GCACGTTGACTAAGGAATGG
RACE_G	CAGATGACCAGGAAATGAAGAG

Table 4

Sequencing primers

Contig.ID	Predicted Position (from start codon)	Forward	Reverse
1	49–800	TCACCTCCAGTACTGAGAACC	TAAAGAAACTTCATCCCACCAG
2	722–1353	AGGTGATCAGTTCATGTTCAG	CTTTCGGGTCCATTTCTTCCT
3	1282–2047	CAGATGACCAGGAAATGAAGAG	GAGCACTTTGGGTATTATATGG
4	1959–2696	TTCTTACAGGGTACTGAGTCCA	AAGTTCACGCTATGCTAAATCC
5	2600–3450	TCTACCACTGAGCTAAATCC	AGTCTTCTTCATTCTTCCCA
6	3404–4206	CCATATGTACAGTGAGTGTCC	TAAATCTGGCCAATGTGATCC
7	4159–4919	TAATTCAAAGGTAGCAGCAG	GTAACCCTAGATCAGAAACAG
8	4864–5660	CCCAGACTCAAACTCACAC	ACCGCCATCATAACATACCC
9	5639–6479	ATGGGTATGTTATGATGGCGG	GTACATTTCATCCTGTGGCT

Table 5

Genomic positions of the extended *CaMK4* 3'UTR

Organism	Chromosome	Start	End
R. norvegicus	Chr 18	25680515	25690671
M. musculus	Chr 18	33185204	33195767
H. sapiens	Chr 5	110820197	110830455

Table 6

RNA-binding protein position weight matrix (PWM) sites mapping to the novel 3'UTR of *CaMK4*.

RNA Binding Protein	PWM Count	RBPDB PWM ID	RBPDB Protein ID
KHDRBS3	169	1174_19561594	1423
ELAVL1 (HuR)	167	1170_19561594	1258
RBMX	152	922_19282290	1487
SFRS1	104	1173_19561594	1448
HNRNPK	78	1217_15351640	1558
HNRNPK	74	1218_15351640	1558
EIF4B	72	352_8846295	1251
SFRS13A	67	1169_19561594	1649
Pum2	58	329_11780640	1800
PABPC1	57	24_7908267	1262
HNRNPK	53	816_15351640	1558
SFRS9	44	797_17548433	1358
MBNL1	42	669_20071745	1507
YTHDC1	38	969_20167602	1283
FUS	25	637_11098054	1289
RBMY1A1	24	1052_17318228	1720
KHSRP	23	1186_17893325	2661
ACO1	14	1213_8021254	2664
NONO	14	488_9001221	1486
RBMY1A1	12	1053_17318228	1720
EIF4B	12	350_8846295	1251
Vts1	11	1176_19561594	2586
PABPC1	11	950_7908267	1262
sap-49	9	145_9163526	2574
ELAVL2 (HuB)	7	783_7972035	1344
QKI	6	1215_16041388	1363
EIF4B	6	351_8846295	1251
a2bp1	6	36_12574126	2570
ELAVL2 (HuB)	4	784_7972035	1344
ybx2-a	3	114_7499328	2571
SNRPA	3	1175_19561594	1274
ZFP36	3	221_12324455	1405
HNRNPA1	3	23_7510636	1444
SNRPA	3	661_1717938	1274
ELAVL2 (HuB)	3	782_8497264	1344

RBPDB = RNA-binding protein database. Note that some gene symbols appear multiple times due to the presence of multiple PWMs for that gene in the RBPDB database.